# Lawrence Berkeley National Laboratory

## Title
THERMAL AND QUANTAL ISOSPIN AND SPIN FLUCTUATIONS IN HEAVY ION REACTIONS

## Permalink
https://escholarship.org/uc/item/7fb70303

## Author
Moretto, L.G.

## Publication Date
1980

Peer reviewed

Invited Paper at the XVIII
International Winter Meeting
on Nuclear Physics, Bormio Italy
January 21-26, 1980

# THERMAL AND QUANTAL ISOSPIN AND SPIN FLUCTUATIONS IN
# HEAVY ION REACTIONS

L. G. Moretto

Nuclear Science
Lawrence Berkeley Laboratory
Berkeley, CA 94720

ABSTRACT

The isobaric charge distributions are discussed in terms of
quantal and classical isospin fluctuations. The roles of mass
asymmetry and of the higher giant isovector modes are treated within
the framework of a cylinder model which is worked out exactly.

Spin fluctuations are considered first in terms of quantal
fluctuations in a cylinder model and second in terms of thermal
fluctuations in a two-sphere model. The results are applied to the
calculation of in- and out-of-plane angular distributions for sequen-
tial fission, alpha and gamma decay. Analytical expressions are
obtained for the angular distributions. The theoretical predictions
are compared with experimental results for sequential fission, alpha
and gamma angular distributions.

INTRODUCTION

Isospin fluctuations have been with us since the halcyon days of
fission, when the chemists used to show their virtuoso performance in
measuring isobaric charge distributions.  Theoreticians did not make
much of it, and the understanding of these distributions did not ex-
tend even to their first moments.  Now, with heavy ion reactions, the
situation has changed somewhat.  On the theoretical side, there are
suggestions that a connection can be made between the charge distribu-
tions and the giant isovector modes of the intermediate complex.  On
the experimental side,  powerful physical techniques are competing
with brave diehard chemists to produce a great variety of charge
distributions as a function of Q-value, mass, excitation energy, etc.
The results look so gloriously messy and, I might venture to say, con-
tradictory, that I could not resist the challenge to add a bit of
theoretical confusion to the experimental one.  This will constitute
the first part of my contribution.

Angular momentum is at present being given a heavy work-out in
compound nucleus studies both in the spectroscopical and in the
continuum γ-ray region.  The results are spectacular, to say the
least, and there is even somebody who claims that they are
understandable as well (always post-factum, of course).

In deep inelastic processes, angular momentum is a fact of of life
and cannot be avoided, although sometimes someone wished he could.
And yet the idea of a spinning intermediate complex has a hidden
fascination of its own.  It is perhaps related to childhood memories,

when spinning toys and similar rotating paraphernalia captured our imagination and intrigued us with their unpredictability and anticommon sense behavior. Be as it may, "rotation is very much in fashion" in heavy ion reactions now-a-days, and the most refined techniques like $\gamma$, $\alpha$, fission fragment angular distributions are applied throughout the world and the periodic table to unravel the mistery of rotating nuclei. Some part of this story both with experimental illustrations and theoretical captions will be told in the second part of this contribution.

A. ISOSPIN FLUCTUATIONS

The mass asymmetry degree of freedom is known to be the slowest to relax among the collective modes excited in heavy ion reactions, while the charge equilibration appears to occur on a faster time-scale.

Information regarding the isospin fluctuations in the intermediate complex can be obtained from the isobaric charge distributions.[1] The observed distributions are Gaussian and the fluctuations can be characterized by the standard derivation $\sigma^2$ of the distributions.

An immediate, though not necessarily warranted approximation has been made by assuming that only the lowest isovector multipole, (corresponding to the E1 mode, like in the giant dipole resonance) is involved in the charge fluctuations.[1,2,3]

If the phonon energy of the dipole mode is $\hbar\omega$ and the stiffness constant is c, then two limiting situations do arise.

The first corresponds to the case in which the collective mode is weakly coupled to the other modes. In this limit and for $T \ll \hbar\omega$ one would expect only ground state quantal fluctuations for which

$$\sigma^2 = \frac{\hbar\omega}{2c} \tag{1}$$

On the other hand, if $T \gg \hbar\omega$ (always weak coupling) or if the collective mode is so strongly coupled to the continuum that its strength function is very spread out, one obtains the classical limit in which the fluctuations depend only upon the temperature $T$:

$$\sigma^2 = \frac{T}{c} \tag{2}$$

It is difficult to argue a priori for either of the two possibilities. If during the decay stage the decoupling from adiabaticity occurs while the neck between the two fragments is still very large and the weak coupling limit holds, one would expect $\hbar\omega \simeq 96/d$ MeV where d is the distance between the two fragment centers. In this case $\hbar\omega \gg T$ in most reactions and large fluctuations, of the order of $\sigma^2 \simeq 1$ $e^2$ should be observed, independent of excitation energy. On the other hand, if the strong coupling limit is prevailing, one would expect fluctuations of perhaps $\sigma^2 \simeq 0.3$ $e^2$ and increasing with excitation energy.

Extraordinarily enough, both situations[2,3] are observed in various reactions as illustrated in Figs. 1 and 2. While this problem, in view of the puzzling experimental data is in a state of substantial confusion, we believe that one should exercise some caution in the assumptions which are commonly made, tacitly or not. In particular the allegedly contradictory findings of large and small charge fluctuations at large and small mass asymmetries respectively,

and the related attempts to infer the relevant E1 phonon energies suffer from a lack of systematic understanding of the role played by the various giant isovector modes in the charge fluctuations.

We are proposing here a simple model[4] that, while it may not be adequately realistic, is complete and points out important facts which have been overlooked.

We shall disregard the extremely important dynamical aspects of the problem[5] and assume that the particular shapes considered in our model just precede the rapid division into two fragments. In particular, let us consider the axial isovector modes in a cylinder of length 2a, radius r, which is suddenly split at a distance b from one of the bases. The standing isovector waves are clearly trigonometric functions and the boundary conditions require them to be cosine functions.

According to the Steinwedel-Jensen model, the fluctuation of the charge density for the mode of order n is:

$$\rho_z = -\frac{1}{2} \rho_z^o a_n \cos k_n x \tag{3}$$

where $\rho_z^o$ is the equilibrium charge density, $a_n$ is the amplitude of the mode, x is the distance along the cylinder axis from one of the bases, and the wave number $k_n$ is given by $k_n = (\pi/2a) n$. The frequency of each mode is given by $\omega_n = k_n u$, where

$$u = \left(\frac{8X}{m} \frac{ZN}{A^2}\right)^{1/2} \simeq 0.21c \tag{4}$$

is the isospin sound velocity, which is assumed to be frequency-independent; $X$ is the liquid drop symmetry energy coefficient and $m$ is the nucleon mass.

If we cut the cylinder at $b$, we can define the charge excess of one of the fragments by the relation:

$$Z_n = \frac{-1}{2} \rho_z^0 a_n \pi r^2 \int_0^b \cos k_n x \, dx = \frac{-a_n Z}{2\pi} \frac{\sin[n\pi Q]}{n} \tag{5}$$

where the degree of symmetry $Q = b/2a$.

Since the transformation from the coordinate $x$ to the variable $Z_n$ does not involve time, we can conclude that $Z_n$ oscillates harmonically, because $a_n$ does. Classically, for a fixed value of $Q$, each $Z_n$ is a separate normal mode.

Let us now determine the stiffness constant of each of these normal modes; we know the frequency already. We can do this by calculating the potential energy (disregarding coulomb forces for the moment):

$$V = X \int \frac{(\rho_n - \rho_z)^2}{\rho_0} d\tau = \frac{X a_n^2}{8} A \tag{6}$$

and substituting the amplitude $a_n$ obtained from Eq. (5) into Eq. (6). The potential energy is indeed quadratic in $Z_n$:

$$V = (1/2) c_n Z_n^2 \text{ with}$$

$$c_n = X \frac{A}{Z^2} \pi^2 \frac{n^2}{\sin^2[n\pi Q]} \tag{7}$$

Note that the stiffness constant depends strongly on n. For any n
some of the charge fluctuations averages out and do not contribute to
the fragment charge fluctuation; this is all the more true the larger
n is, since it takes more energy to displace a given amount of charge
into any given fragment. Even for the lowest mode ($n = 1$), some of
the energy goes into polarizing the fragments rather than displacing
charge. This is to be contrasted with the standard way in which c has
been calculated so far, using a potential which neglects fragment
polarization: $V = V_{LD}(1) + V_{LD}(2) + V_C(1,2)$ where $V_{LD}(1)$ and $V_{LD}(2)$
are the liquid drop energies of two touching spheres and $V_C(1,2)$ is
their Coulomb repulsion. The stiffness constant follows as:

$$c_{LD} = \left. \frac{\partial^2 V}{\partial Z_1^2} \right|_{\text{constant } A} \tag{8}$$

where $Z_1$ is the charge of one of the fragments. In Fig. 3, $c_1$ and
$c_{LD}$ can be compared as a function of Q. The large error introduced
by neglecting the fragment polarization is obvious, especially at
large asymmetries.

Notice also that for the special values of Q for which $\sin[n\pi Q]$ is
zero, the stiffness constant is infinite; no matter how much work is
done, no charge displacement arises. This is true in particular at
symmetry ($Q = 1/2$), where none of the even modes contribute to
displacement.

After having identified the $Z_n$ as classical normal modes, we can immediately quantize them. For each mode we obtain a phonon energy:

$$\hbar\omega_n = \frac{\hbar u \pi}{2a} \, n \tag{9}$$

These phonon energies are very large even for the lowest modes, so that the limit $T/\hbar\omega_n \ll 1$ is typically encountered ($T \cong$ nuclear temperature) and only zero-point fluctuations need to be considered.

For each mode $n$ the zero-point charge width is given by:

$$\sigma_n^2 = \frac{\hbar\omega_n}{2c_n} = \sigma_1^2(\text{symmetry}) \, \frac{\sin^2[n\pi Q]}{n} \tag{10}$$

From Fig. 3 and Eq. (8), one expects these widths to be smaller at large asymmetries than those calculated neglecting fragment polarization, and experiment[2,3] indicates such an effect. The contribution of the nth mode to $\sigma^2$ goes like $1/n$, so that the contribution of the higher modes becomes less relevant the higher $n$ is. However, the total charge width in this model diverges logarithmically:

$$\sigma^2 = \sigma_1^2(\text{symmetry}) \, \sum \frac{\sin^2[n\pi Q]}{n} \tag{11}$$

This is not surprising because we are assigning an infinite number of degrees of freedom to a system of finite particle number. Furthermore, it is likely that the higher-frequency modes "drown" in the doorway states directly coupled to them, as illustrated in[1] thus

removing the collectiveness from the respective degrees of freedom. The location of the cutoff in n, or even whether a fully quantal treatment is warranted for the lowest mode, is most relevant.

The wavelength of the oscillations cannot be much smaller than the diameter of a nucleon; thus one obtains the following cutoff in n: $n_{max} = 4.8 \, A^{1/3}$ for $\lambda_{min} = 1.5$ fm.

A very important feature of this model is that the role of each mode strongly depends upon the asymmetry of the system. In Fig. 4(a) the normalized partial width is given as a function of asymmetry for a few values of n, in Fig. 4(b), they are given as a function of n for a few asymmetries. At values close to symmetry, the lowest mode dominates, but with increasing asymmetry the higher n modes play an ever increasing role. The widths are zero when a half-multiple of the wavelength for a mode matches the value of b. In Fig. 5 the width arising from the first n modes is given for a few n values as a function of Q. This shows that an experimentally observed width, especially in asymmetric systems may include the comparable contribution of several modes.

It is clear that any attempt to relate such width to a single E1 mode rather than to the combination of several isovector modes may be doomed to failure. The difficulties are compounded by the use of a stiffness constant which may dramatically depend on the form of the standing wave and which has been calculated incorrectly so far even for the lowest mode. The cylindrical geometry is likely to be a poor approximation, but the introduction of a neck to better simulate the

separation of the fragments leads to complications which may involve non-linear and dispersive effects. Dynamics is especially important, since the salient feature of this problem is the configuration associated with the neck snapping.

In conclusion, information on the isovector modes from the measurement of the charge fluctuation at high temperatures can only be obtained by properly accounting for both the effect of mass asymmetry and the role of higher order modes.

B.  ANGULAR MOMENTUM TRANSFER

The interactions between two colliding nuclei, especially those associated with short range forces, both conservative and dissipative, create strong torques responsible for transfer of angular momentum from orbital motion to intrinsic rotation of the fragments. The magnitude of the transferred angular momentum can be determined in various ways. The measurement of the $\gamma$-ray multiplicity is one such method of quite general application. By this technique, the angular momentum transfer has been studies as a function of Q value and of exit-channel mass asymmetry.

The general rise of the multiplicity with increasingly negative Q values (Fig. 6) is attributed mainly to the progressive tendency towards the rigid rotation limit expected as the $\zeta$ value and the interaction times increase.[6]  The V shaped dependence of the $\gamma$-ray multiplicity upon mass asymmetry (Fig. 7) in the quasi elastic region[7] is interpreted as a general tendency to transfer angular momentum with transferred mass on one hand, and as due to an increased

Q value observed with increased net mass transfer on the other. Of course if energy is transferred only through mass exchange, the two explanations are identical.

In the deep inelastic region two extreme cases have been observed. In the first case, when a narrow l-window is available for deep inelastic products, a multiplicity rising with increasing asymmetry is observed[8,9] in agreement with the rigid rotation limit, as shown in Fig. 8. In the second case, when a very large l window is available, the $\gamma$-ray multiplicity is essentially constant as a function of mass asymmetry. Examples of this case are readily available in the Kr-induced reactions[7] shown in Fig. 9. The accepted explanation of this behavior is an angular momentum fractionation along the mass asymmetry coordinate. Since large l-waves are associated with short lifetimes and vice-versa, small l-waves populate prevalently the large asymmetries, far removed from the entrance channel asymmetry. In this way the tendency of $\gamma$-ray multiplicities to increase with increasing asymmetry, as required by rigid rotation is more or less compensated by the progressive decrease of the average angular momentum. All these effects are reasonably well understood on a more quantitative theoretical ground, as shown in Figs. 6 and 10 where the results of a diffusion model calculation are shown.[6]

Angular Momentum Fluctuations

Hints of fluctuations in the fragment spins have been seen in the second moment of the $\gamma$-ray multiplicities.[10] However, a much better indicator of spin fluctuations is the degree to which the

fragment spins are misaligned. This misalignment, as we shall see, can be readily detected by measuring the angular distributions of γ-rays, α particles, fission fragments emitted from the primary deep inelastic fragments. The origin of these fluctuations can be quantal or classical, and can be due either to non equilibrium or equilibrium processes. Let us consider first one example of equilibrium quantal fluctuations and examples of thermal fluctuations later on.

Quantal Effects

In view of the analogy between spin and isospin we can take advantage of the cylinder model results obtained in the previous section.

Instead of neutron and proton fluids, we consider now two new nucleon fluids, one with positive and the other with negative spin projection on the cylinder axis.

Let us assume that the density of the doubly degenerate single particle levels is g and that the average spin projection of each particle on the cylinder axis is M. Then n aligned broken pairs will generate an angular momentum:

$$I = 2nM \tag{12}$$

and an energy:

$$U = \frac{n^2}{g} \tag{13}$$

wnich leads to the relation:

$$U = \frac{I^2}{4M^2 g} = \frac{I^2}{2\mathcal{J}}$$ (14)

where $\mathcal{J} = 2M^2 g$ is the moment of inertia of the cylinder.

In analogy with the symmetry energy we can write the rotational energy $U$ as:

$$U = x_I \frac{I^2}{A} \quad \text{with} \quad x_I = \frac{A}{2\mathcal{J}}$$ (15)

Now a perturbation consisting in a variation of the angular velocities of contiguous perpendicular slices of the cylinder will move with a velocity (spin velocity):

$$u^2 = 8x_I \frac{\rho_0^+ \rho_0^-}{m \rho_0^2} \cong 2 \frac{x_I}{m}$$ (16)

where $\rho_0^+$, $\rho_0^-$, $\rho_0$ are the equilibrium densities of right-handed, left-handed and total fluid, and $m$ is the nucleon mass.

The eigen modes are defined as in the case of isospin. Their quantization leads to the phonon energies:

$$\hbar\omega_n = \frac{\hbar u \pi}{2a} n$$ (17)

a being the half-length of the cylinder and n the order of the mode.

The stiffness constants are:

$$c_n = \frac{4\pi^2 \chi_I}{A} \frac{n^2}{\sin^2[n\pi Q]} \tag{18}$$

$Q$ being the asymmetry of the cut as in the previous section.

The widths are:

$$\sigma_n^2 = \sigma_1^2(\text{symmetry}) \frac{\sin^2[n\pi Q]}{n} \tag{19}$$

where

$$\sigma_1^2(\text{symmetry}) = \frac{\hbar\omega_1}{c_1} = \frac{\hbar}{8\pi a} \sqrt{\frac{A\ell}{m}} \tag{20}$$

For a cylinder approximating two equal touching spheres and for $A = 200$ the width of the lowest mode is

$$\sigma_1(\text{symmetry}) \simeq 1.7\hbar$$

As we shall see this quantal width is negligible as compared to that expected from thermal fluctuations.

## Statistical Excitation of Angular Momentum Bearing Modes

Let us consider a frame of references where the z axis is parallel to the entrance-channel angular momentum, the x axis parallel to the recoil direction of one of the fragments, and the y axis perpendicular to the z,x plane.

A misalignment of the fragment angular momentum arises when non-vanishing x and y components of the fragment angular momentum are

present. Among the possible sources of these components, the thermal excitat⁊ of angular momentum–bearing modes of the intermediate complex appears very likely and can be readily investigated.

If the intermediate complex is assumed to have the shape of two equal touching spheres, the angular momentum bearing normal modes are easily identifiable. In Fig. 11 and Fig. 12 these modes are illustrated. We shall call them "bending," B (doubly degenerate), "twisting" Tw (degenerate with bending), "wriggling" W (doubly degenerate) and "tilting" Ti.

In a recent work, the statistical mechanical aspects of the excitation of these modes has been studied in detail.[11] Here we report only the relevant conclusions.

The thermal excitation of these collective modes leads to Gaussian distributions in the three components $I_x$, $I_y$, $I_z$, namely:

$$P(\underset{\sim}{I}) \quad \exp - \left[ \frac{I_x^2}{2\sigma_x^2} + \frac{I_y^2}{2\sigma_y^2} + \frac{(I_z - \bar{I}_z)^2}{2\sigma_z^2} \right] \tag{21}$$

where:

$$\sigma_x^2 = \sigma_{Tw}^2 + \sigma_{Ti}^2 = \frac{1}{2}\mathscr{J}T + \frac{7}{10}\mathscr{J}T = \frac{6}{5}\mathscr{J}T$$

$$\sigma_y^2 = \sigma_B^2 + \sigma_W^2 = \frac{1}{2}\mathscr{J}T + \frac{5}{14}\mathscr{J}T = \frac{6}{7}\mathscr{J}T \tag{22}$$

$$\sigma_z^2 = \sigma_B^2 + \sigma_W^2 = \frac{1}{2}\mathscr{J}T + \frac{5}{14}\mathscr{J}T = \frac{6}{7}\mathscr{J}T \quad .$$

The quantity $\mathcal{J}$ is the moment of inertia of one of the two touching

spheres, and T is the temperature.

## Angular Distributions of Sequential Fission and of Sequential Light Particle Emission

The magnitude of the angular momentum misalignment can be measured

through the in and out-of-plane angular distribution of the decay

products of one of the two fragments. We h. : shown elsewhere that

the angular distribution of fission fragments and of light particles

emitted by a compound nucleus can be treated within a single

framework.[12]

The direction of emission of a decay product (fission fragment,

$\alpha$-particle, etc) is defined by the projection K of the fragment

angular momentum on the disintegration axis. Simple statistical

mechanical considerations show that the distribution in K values is

Gaussian. More precisely, the decay width is given by:

$$\Gamma^{I} = \Gamma^{0} \exp\left[-\frac{\hbar^2 I^2}{2T}\left(\frac{1}{\mathcal{J}_1} - \frac{1}{\mathcal{J}_c}\right)\right]\exp - K^2/2K_0^2 \tag{23}$$

This distribution in K determines the angular distribution:

$$\Gamma^{I} \propto \exp - (\underset{\sim}{I}\cdot\underset{\sim}{n})^2/2K_0^2 \tag{24}$$

where $\underset{\sim}{n}$ is a unit vector pointing in the decay direction.

The dot product $\underset{\sim}{I}\cdot\underset{\sim}{n}$ can be explictly written down:

$$\underline{I} \cdot \underline{n} = I_x \sin\theta \cos\phi + I_y \sin\theta \sin\phi + I_z \cos\theta \tag{25}$$

Assuming the statistical distribution[21] one can obtain the angular distribution for any given I by integrating over $I_x$, $I_y$, $I_z$:[17]

$$\bar{\Gamma}^I \propto \frac{1}{S(\theta,\phi)} \exp - \frac{I_z^2 \cos^2\theta}{2S^2(\theta,\phi)} \tag{26}$$

where

$$S^2(\theta,\phi) = K_0^2 + (\sigma_x^2 \cos^2\phi + \sigma_y^2 \sin^2\phi) \sin^2\theta + \sigma_z^2 \cos^2\theta \tag{27}$$

Integration over the fragment angular momentum distribution, assumed to reflect the entrance channel angular momentum distribution through the rigid rotation condition, leads to the following expression:

$$W(\theta,\phi) = \int_a^{I_{max}} 2I \, dI \int_{-I}^{+I} dK \, \frac{\Gamma^I(K)}{\Gamma_T^I} \tag{28}$$

If $\Gamma_T = \Gamma_N$

$$W(\theta,\phi) \propto \int_0^{I_{max}} \frac{2I}{S} \exp - I_z^2 \left[ \frac{\cos^2\theta}{2S^2} - \beta \right] \, dI \tag{29}$$

or

$$W(\theta,\phi) = \frac{1}{SA} [1 - \exp(-A)] \tag{30}$$

where

$$A = I_{max}^2 \left( \frac{\cos^2 \theta}{2S^2} - \beta \right) \tag{31}$$

$$\beta = \frac{\hbar^2}{2T} \left( \frac{1}{\mathscr{J}_n} - \frac{1}{\mathscr{J}_\perp} \right)$$

The quantity $\mathscr{J}_n$ is the moment of inertia of the nucleus after neutron emission, $\mathscr{J}_\perp$ is the perpendicular moment of inertia of the critical shape for the decay (e.g., saddle point).

It is important to notice that the angular momentum dependence of the particle/neutron competition or fission/neutron competition is taken into account through $\beta$. This point seems to have been neglected in recent work on sequential decay. The final ingredient necessary for an explicit calculation of the angular distributions is the quantity $K_0^2$. This quantity can be expressed in terms of the principal moments of inertia of the critical configuration for the decay:

$$K_0^2 = \frac{1}{\hbar^2} \left( \frac{1}{\mathscr{J}_\parallel} - \frac{1}{\mathscr{J}_\perp} \right)^{-1} T = \mathscr{J}_{eff} T \tag{32}$$

For fission $\mathscr{J}_{eff}$ can be taken from the liquid drop calculations of C.P.S.[13]

For lighter particle emission, the calculation of $\mathscr{J}_{eff}$ can be worked out trivially. Let $m$, $M$, $A$ be the masses of the light, residual and total nucleus. One obtains:

$$\mathcal{J}_\parallel = \frac{2}{5} MR^2 + \frac{2}{5} mr^2$$

$$\mathcal{J}_\perp = \frac{2}{5} MR^2 + \frac{mM}{A} (R + r)^2 \qquad (33)$$

$$\frac{\mathcal{J}_{eff}}{\mathcal{J}_{sph}} = \left(\frac{M}{A}\right)^{5/3} \left[1 + \frac{2}{5} \frac{A}{m} \left(\frac{R}{R + r}\right)^2\right]$$

where r and R are the radii of the light particle and residual nucleus respectively.

Now we are in the position to calculate both in-plane and out-of-plane anisotropies.

The in plane anisotropy gives:

$$\frac{W(\phi = 90°)}{W(\phi = 0°)}\bigg|_{\theta=90°} = \left(\frac{K_0^2 + \sigma_x^2}{K_0^2 + \sigma_y^2}\right)^{1/2} \qquad (34)$$

Since in most cases $K_0^2$ is fairly large, or at least comparable with $\sigma_x^2$ or $\sigma_y^2$ it is difficult to obtain a sizable in-plane anisotropy. Even by letting $\sigma_x = 0$ one needs $\sigma_y^2 = 3 K_0^2$ just to obtain the anisotropy of 2! The out-of-plane anisotropy is somewhat more complicated:

$$\frac{W(\theta = 90°)}{W(\theta = 0°)}\bigg|_{\phi=0°} = \frac{1}{\beta}\left(\frac{K_0^2 + \sigma_z^2}{K_0^2 + \sigma_x^2}\right)^{1/2} \left(\beta - \frac{1}{2(K_0^2 + \sigma_z^2)}\right) \qquad (35)$$

$$\times \frac{1 - \exp\beta I_{max}^2}{1 - \exp I_{max}^2\left(\beta - \frac{1}{2(K_0^2 + \sigma_z^2)}\right)}$$

At $\phi = 90°$ the anisotropy is obtained from the above equation by interchanging $\sigma_x$ with $\sigma_y$. A calculation of in-plane and out-of-plane sequential fission angular distributions is shown in Fig. 13 for the reaction Kr + Au at 600 MeV. The in-plane anisotropy has been created by artificially setting $\sigma_x = 0$.

In Fig. 14 the experimental width of the out-of-plane distribution for the same reaction is shown.[14]

In Fig. 15 the theoretical calculation, again for the same reaction indicates an excellent agreement with experiments.

Sequential α Decay

In Fig. 16 the out-of-plane angular distributions for sequential α decay from Ag-like fragments are shown for the reaction 664 MeV Kr + Ag. In order to show the sensitivity to misalignment, the angular distribution is also calculated assuming $\sigma_x = \sigma_y = \sigma_z = 0$. Experimental kinetic energy spectra for the α-particles emitted by Ag at different out-of-plane angles are shown in Fig. 17. These spectra are in the frame of the recoiling Ag and indicate that we are indeed dealing with evaporation.

In Fig. 18 the Q value and $l$ dependence of the experimental angular distribution are shown. The Q value dependence is understandable as follows. In the lower part of the Q value spectrum (higher fragment kinetic energies) one has contribution from the higher l-waves, while in the higher part of the Q value spectrum as one moves towards the Coulomb barrier and below, the main contribution is expected to come from the low l-waves. As a consequence, with

progressively increasing Q value the ratio $\sigma^2/I^2$ increases and the angular distributions become less sharp. The increase of the anistropy with decreasing fragment atomic number can be understood from the rigid rotation condition. As the splitting becomes more asymmetric, a larger fraction of the total angular momentum goes into fragmen spin, and the larger fragment (Ag-like fragment) gets the larger part of it (the fragment spins are in the ratio $(A_1/A_2)^{5/3}$). Consequently, as the Z of the detected fragment is lowered, the spin of the Ag-like fragment increases and the anistropy of the alpha particles emitted by it increases accordingly.

In Fig. 19 the use of a $\gamma$-ray multiplicity filter snows that the angular distribution becomes sharper when a larger number of $\gamma$-rays are required to be in coincidence with the $\alpha$-particle. This effect is readily understood since a large $\gamma$-ray multiplicity indicates large angular momentum which in turn implies a smaller misalignment.

A detailed analysis of these data has not been performed as yet.

Gamma ray angular distributions

Fragments with large amounts of angular momentum are expected to dispose of it mainly by stretched E2 decay. The relative amounts of dipole and quadrupole radiation depends mainly upon the ability of the nucleus to remain a good rotor over the whole angular momentum range.

If the angular momentum of the fragment is aligned, the typical angular pattern of the quadrupole radiation should be observed. Any misalignment should decrease the sharpness of the angular distribution.

If the distribution of the angular momentum components $I_x$, $I_y$, $I_z$ is statistical, it is straightforward to derive analytical expressions for the angular distributions.

For a perfectly aligned system we have:

$$W(\alpha) = \frac{3}{4} (1 + \cos^2\alpha) \quad ; \quad W(\alpha) = \frac{5}{4} (1 - \cos^4\alpha) \qquad (36)$$

$$\text{for El} \qquad\qquad\qquad \text{for E2}$$

If the angular momentum is not aligned with the z axis, one must express $\alpha$ in terms of $\theta$, $\phi$ which define the direction of the angular momentum vector. In particular we have:

$$\cos\alpha = \frac{\underline{I} \cdot \underline{n}}{I} = \frac{I_x \sin\theta \cos\phi + I_y \sin\theta \sin\phi + I_z \cos\theta}{(I_x^2 + I_y^2 + I_z^2)^{1/2}} \qquad (37)$$

For any given I, the angular distribution is obtained by integration over the statistical distribution $P(\underline{I})$ of the angular momentum components:

$$W(\theta,\phi) = \int W(\alpha) \ P(\underline{I}) \ d\underline{I} \qquad (38)$$

It is not possible to obtain exact analytical expression. However, an expansion to order $\sigma_x^2/\bar{I}_z^2$, $\sigma_y^2/\bar{I}_z^2$, etc. is adequate and expressions can be obtained in closed form.

For the dipole decay we have:

$$W(\theta,\phi) = \frac{3}{4}(1 - \cos^2\theta) + \frac{3}{4}\left[(\sin^2\theta \cos^2\phi - \cos^2\theta)\frac{\sigma_x^2}{\bar{I}_z^2}\right.$$

$$\left. + (\sin^2\theta \sin^2\phi - \cos^2\theta)\frac{\sigma_y^2}{\bar{I}_z^2}\right] \tag{39}$$

Notice that there is no dependence upon $\sigma_z^2$. In the case in which $\sigma_x = \sigma_y = \sigma$, we obtain the simplified expression:

$$W(\theta,\phi) = \frac{3}{4}(1 + \cos^2\theta) + \frac{3}{4}(\sin^2\theta - 2\cos^2\theta)\frac{\sigma^2}{\bar{I}_z^2} \tag{40}$$

A weak in-plane anisotropy is possible:

$$\frac{W(\phi = 0^\circ)}{W(\phi = 90^\circ)}\bigg|_{\theta=90^\circ} = \frac{1 + \sigma_x^2/\bar{I}_z^2}{1 + \sigma_y^2/\bar{I}_z^2} \cong 1 + \frac{\sigma_x^2 - \sigma_y^2}{\bar{I}_z^2} \tag{41}$$

The out-of-plane anisotropy is:

$$\frac{W(0^\circ)}{W(90^\circ)} = 2\frac{(1 - \sigma^2/\bar{I}_z^2)}{(1 + \sigma^2/\bar{I}_z^2)} \approx 2(1 - 2\sigma^2/\bar{I}_z^2) \tag{42}$$

For the quadrupole decay we have:

$$W(\theta,\phi) = \frac{5}{4}(1 - \cos^4\theta) - \frac{5}{2}\left[\left(3\sin^2\theta\cos^2\theta\cos^2\phi - \cos^4\theta\right)\frac{\sigma_x^2}{\bar{I}_z^2}\right. \quad (43)$$

$$\left. + (3\sin^2\theta\cos^2\theta\sin^2\phi - \cos^4\theta)\frac{\sigma_y^2}{\bar{I}_z^2}\right]$$

Again, no dependence upon $\sigma^2$ is predicted. If one assumes $\sigma_x = \sigma_y = \sigma$ as before, one obtains:

$$W(\theta) = \frac{5}{4}(1 - \cos^4\theta) - \frac{5}{2}(3\sin^2\theta\cos^2\theta - 2\cos^4\theta)\,\sigma^2/\bar{I}_z^2 \quad (44)$$

and

$$\frac{W(0°)}{W(90°)} \approx 4\frac{\sigma^2}{\bar{I}_z^2} \quad (45)$$

For the in plane anisotropy we have:

$$\left.\frac{W(\phi = 0°)}{W(\phi = 90°)}\right|_{\theta=90°} \sim 1 \quad (46)$$

to order $\sigma^2/\bar{I}_z^2$. This can be easily understood. The rms misalignment is $\sim\sigma/\bar{I}$, thus, at $\theta = 90°$:

$$W(90) = 1 - \cos^4\left(90° - \frac{\sigma}{\bar{I}}\right) \approx 1 - \frac{\sigma^4}{I^4} \quad (47)$$

Thus, no second order term exists. This result shows that its is impossible to study anistropies in the angular momentum misalignment by means of $\gamma$-ray angular distribution.

These results are summarized in ig. 20 where the anisotropy is plotted as a function of the fraction of El radiation for various values of $\sigma^2/\bar{I}^2$. If one has a fairly good experimental idea of the amount of El radiation to be expected from a given fragment, the measurement of the anistropy yields directly the value of $\sigma^2/\bar{I}^2$, which is of course the most direct information about the misalignment.

The 1060 MeV Xe + Au Experiment[15]

The predictions of the model just described can be compared with the $\gamma$-ray anistropy measured for the above system.[15] A window in mass was set in the neighborhood of symmetric splitting, in order to consider fragments in the heavy rare-earth region which are good rotors and for which the amount of dipole radiation has been measured to be ~20 percent. The temperature of the system at symmetry is estimated to be $T \simeq 2$ MeV, and

$$\sigma^2 \cong \frac{\mathcal{J}_T}{\hbar^2} = 140 \quad .$$

In the absence of angular momentum fractionation, the rms fragment spin should be $I_F \simeq 46\hbar$. However, the measured $\gamma$-ray multiplicity yields $I \simeq 32\hbar$ indicating that fractionation occurs along the mass asymmetry coordinate and that the lower l-waves have a better chance to reach symmetry. Thus the misalignment parameter is $\sigma^2/\bar{I}^2 \simeq 0.14$. With 20 percent El transitions, Fig. 20 predicts antisotropies close to 0.70. The experimental results, shown in Fig. 21 indicate that

such an anisotropy is indeed observed in the region of gamma ray
energies where the quadrupole bump is observed.

The 1400 MeV $^{165}$Ho + $^{165}$Ho experiment.[16]

In this experiment the most probable exit channel is already
symmetric and in the mass region where a good rotor behavior is well
established. Angular momentum fractionation is not expected to occur
due to the strong concentration of the cross section near symmetric
splitting. The temperature is estimated to be $T \simeq 2.1$ MeV and the rms
fragment spin is $I_F = 52\hbar$, leading to a misalignment parameter $\sigma^2/\bar{I}^2 = 0.055$.
With 20 percent E1 one would expect anisotropies of ~0.4 or their
reciprocal in excess of 2. An inspection of the gamma-ray spectra
(Fig. 22) shows that at 90° out-of-plane no quadrupole bump is
observed, while in-plane a strong quadrupole bump is visible. In the
region of the bump, the anisotropy reaches values higher than 2, while
in the region above the bump the anisotropy disappears (Fig. 23).
Thus one can conclude that the system is strongly aligned and that the
misalignment is close to that predicted by the statistical model. A
remarkable dependence of the anisotropy upon Q value is also observed,
the anisotropy being largest at intermediate Q values. This pheno-
menon is readily explained. At small inelasticities, little angular
momentum is transferred to the fragments. Thus the amount of
quadrupole radiation is small, while that of dipole should be almost
independent of Q value. Thus weak anisotropies should be expected.
At intermediate inelasticities a large amount of angular momentum is
transferred and a large amount of quadrupole rotation is emitted while

the misalignment parameter $\sigma^2/\bar{I}^2$ is relatively small. This
results in large anistropies. At the largest inelasticities only the
lowest 1-waves are known to contribute. Thus $\sigma^2/\bar{I}^2$ becomes
larger and the anisotropies are weaker.

## CONCLUSION

Someone of my 25 listeners (and readers), if that many have
negotiated this long trek with me, may still be curious as to what the
connection may be between the isospin and the spin part of my talk.
Frankly, I would rather not answer directly such a question. Perhaps
it may suffice to say that like many other colleagues, I am inordi-
nately enjoying both subjects. And it may be worth meditating again
on this beautiful toy that the nucleus is, so flexible and multi-
faceted to span micro and macrophysics, moving from spectroscopical to
statistical regimes with an ease and an open mind that some of us
observers may have not mastered quite yet.

REFERENCES

1) L. G. Moretto, J. Sventek and G. Mantzonuranis, Phys. Rev. Lett. 42 (1979) 563.

2) G. Wirth, W. Brüchle, H. Gäggeler, J. V. Kratz, M. Schädel, I. Warneke, G. Hermann, M. Weis, R. Lucas, J. Poitou, Hizschegg (1979) p. 13.

3) M. Berlanger, A. Gobbi, F. Hanappe, V. Lynen, C. Ngô, A. Olmi, H. Sann, H. Steltzer, H. Richel and M. F. Rivet., Z. Physik A291 (1979) 133. See also C. Ngô, these proceedings.

4) L. G. Moretto, C. R. Albiston and G. Mantzouranis, Lawrence Berkeley Laboratory preprint LBL-9896, November 1979.

5) See for instance H. Nifenecker, preprint.

6) R. Reginbart, A. Behkami, G. J. Wozniak, R. P. Schmitt, J. J. Sventek, and L. G. Moretto, Phys. Rev. Lett. 41, (1978) 1355.

7) M. M. Aleonard, G. J. Wozniak, P. Glässel, M. M. Deleplanque, R. M. Diamond, L. G. Moretto, R. P. Schmitt and F. S. Stephens, Phys. Rev. Lett. 40, (1978) 622.

8) P. Glässel, R. S. Simon, R. M. Diamond, R. C. Jared, I. Y. Lee, L. G. Moretto, J. O. Newton, R. Schmitt and F. Stephens, Phys. Rev. Lett. 38 (1977) 331.

9) J. B. Natowitz, N. M. Namboodiri, P. Kasiraj, R. Eggers, L. Adler, P. Goutier, C. Cerutti and T. Alleman, Phys. Rev. Lett. 40 (1978) 751.

10) P. Christensen, F. Folkmann, O. Hansen, O. Nathan, N. Trautner, F. Videbaeck. S. Y. van der Werf, H. C. Britt, R. P. Chestnut, H. Freiesleben, and F. Pulhofer, Phys. Rev. Lett. 40 (1978) 1245.

11) L. G. Moretto and R. P. Schmitt, Phy. Rev. C21 (1980) 204.

12) L. G. Moretto, Nucl. Phys. A247 (1975) 211.

13) S. Cohen, F. Plasil, and W. J. Swiatecki, Ann. Phys. (NY) 82 (1974) 557.

14) G. J. Wozniak, R. P. Schmitt, P. Glässel, R. C. Jared, G. Bizard, and L. G. Moretto, Phys. Rev. Lett 40 (1978) 1436.

15) P. Aguer, G. J. Wozniak, R. P. Schmitt, D. Habs, R. M. Diamond, C. Ellegaard, D. L. Hillis, C. C. Hsu, G. J. Mathews, L. G. Moretto, G. U. Rattazzi, C. P. Roulet, and F. Stephens, Phys. Rev. Lett. 43 (1979) 1778.

16) Collaboration between Moretto and Diamond-Stephens groups. Preliminary data.

17) R. A. Broglia, G. Pollarolo, C. H. Dasso and T. Døssing, Phys. Rev. Lett. 43 (1979) 1649.

FIGURE CAPTIONS

Fig. 1)  Variances of the $Z$ distributions at fixed mass asymmetry vs. excitation energy in the reaction $^{136}$Xe + Au.  The dashed and solid curves indicate the expected variance from quantal and classical statistical fluctuations.[2]

Fig. 2)  Widths of the $Z$ distributions for several masses vs. total kinetic energy for the reaction $^{86}$K + $^{98}$Mo.[3]

Fig. 3)  The stiffness constant for the oscillation of the charge excess is plotted against asymmetry ($Q = A_1/A_{total}$) for $A = 100$.  The dashed curve corresponds to the liquid drop potentials for two touching spheres.  The solid curve corresponds to the cylinder model for the lowest mode.  The Coulomb term is included in both calculations.[4]

Fig. 4)  The square of the normalized partial width is plotted a) against asymmetry at fixed n; b) against n at fixed asymmetry.[4]

Fig. 5)  The sum of the squares of the normalized partial widths up to $n_{max}$ is plotted against asymmetry.[4]

Fig. 6)  Gamma ray multiplicity vs. total kinetic energy for three Kr induced reactions.  The solid and dashed curves are fit to the data.[6]

Fig. 7)  Gamma ray multiplicities vs. $Z$ for the quasi elastic components of the reactions $^{165}$Ho, $^{197}$Au + 618 MeV $^{86}$Kr.[7]

Fig. 8)  Gamma ray multiplicities for the reaction 175 MeV $^{20}$Ne + Ag at 90° Lab,[8] and for the reaction 237 MeV $^{40}$Ar + $^{89}$Y.

Fig. 9)  Gamma ray multiplicities vs. Z for the deep inelastic compo-
nents in 618 MeV $^{86}$Kr + $^{nat}$Ag, $^{165}$Ho, $^{197}$Au.[7]

Fig. 10) Gamma ray multiplicity vs. Z for three reactions.  The open
circles represent the quasi elastic components and the solid
circles the deep inelastic components.  Solid curves are fit
to the data.[6]

Fig. 11) Schematic illustration of the tilting (Ti) mode and of the
doubly degenerate wriggling (W) mode.  The long arrow origi-
nating at the point of tangency is the orbital angular momen-
tum, while the shorter arrows represent the individual
fragment spins.[11]

Fig. 12) Schematic illustration of the twisting (Tw) and of the doubly
degenerate bending (B) modes.  Notice the pair-wise cancella-
tion of the fragment spins.[11]

Fig. 13) In-plane and out-of-plane angular distribution for sequential
fission in the reaction 600 MeV Kr + Au.  The in-plane
anistropy is generated by explicitly setting $\sigma_x = 0$.

Fig. 14) Full width at half maximum of the out-of-plane fission and
non-fission components as a function of Z in the reaction
618 MeV $^{86}$Kr + $^{197}$Au.[14]

Fig. 15) Calculated out-of-plane sequential fission angular distribu-
tion of the reaction 620 MeV $^{86}$Kr + $^{197}$Au.

Fig. 16) Calculated out-of-plane angular distribution for sequential
alpha decay from the Ag-like fragment in the reaction 664 MeV
$^{84}$Kr + $^{nat}$Ag (dashed line).  The solid line has been
obtained by setting $\sigma = 0$.

Fig. 17) Kinetic energy spectra at various out-of-plane angles for the alphas evaporated from the Ag-like fragment in the reaction 664 MeV $^{84}$Kr + $^{Nat}$Ag. The spectra are in the center-of-mass of the Ag-like fragment.

Fig. 18) Q-value and Z dependence of the alpha particle out-of-plane distribution for the same reaction as in Fig. 16.

Fig. 19) Dependence of the alpha out-of-plane angular distribution upon the gating on various folds in the gamma multiplicity filter.

Fig. 20) Calculated out-of-plane gamma ray anistropies as a function of the %E1 for various values of $\sigma^2/\bar{I}^2$.

Fig. 21) (Please observe only left-hand side) Out-of-plane gamma ray anistropy as a function of gamma ray energy for the reaction 1064 MeV $^{136}$Xe + Au in the product mass range $152 < A < 172$ at three different Q-value bins.

Fig. 22) a, b  In plane gamma ray pulse-height spectra for the reaction 1400 MeV $^{165}$Ho + $^{165}$Ho for different Q bins. In the first bin, the quadrupole bump is absent. The 90° out-of-plane pulse height spectrum closely resembles the in-plane spectrum for the first bin at all Q values.

Fig. 23) a, b  Out-of-plane gamma ray anistropies for the same reaction and Q value bins as in Fig. 22 as a function of gamma ray energies.
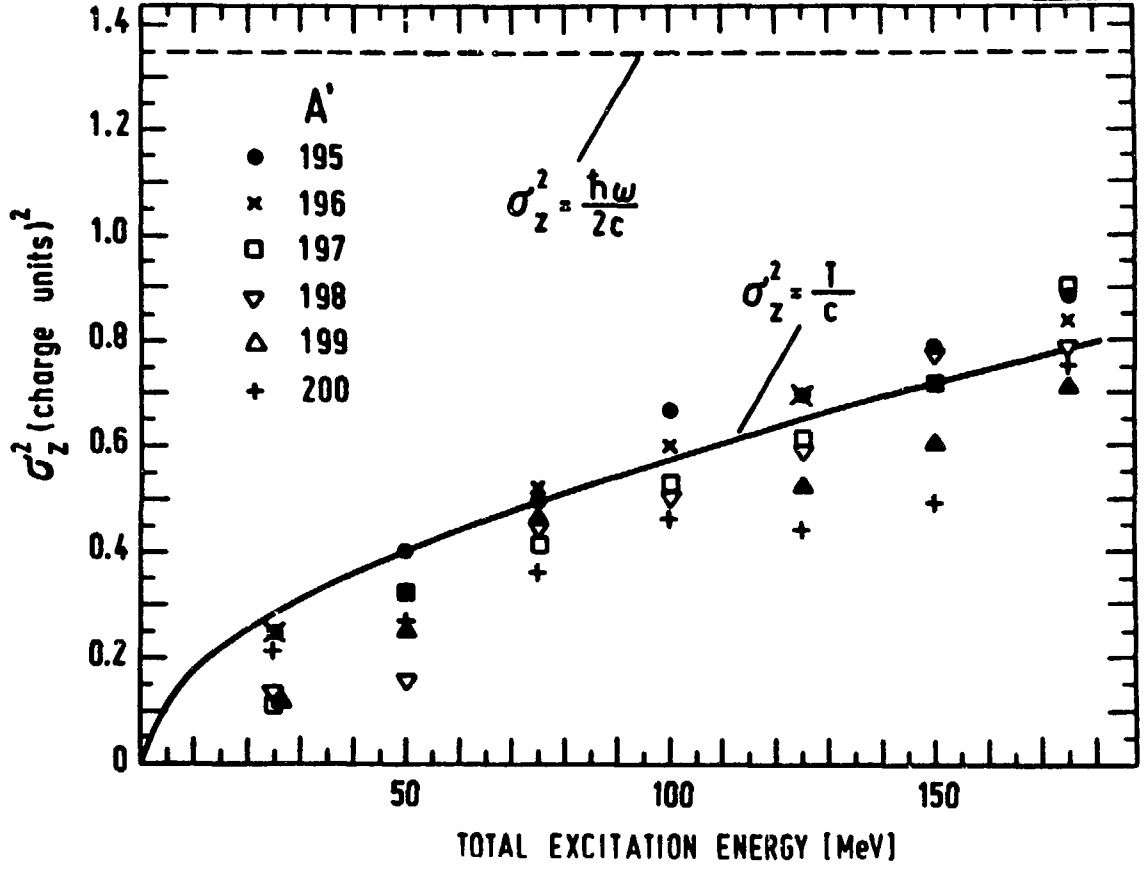
Figure 1
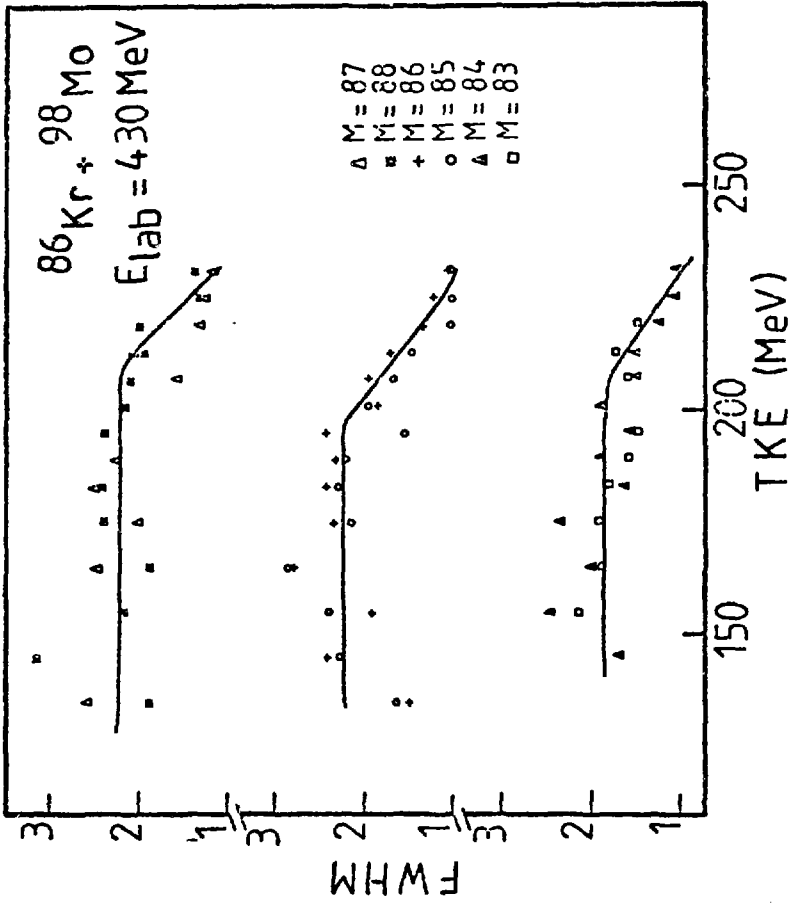
Figure 2

XBL 7910-4422

Figure 3

$q_n^2/q_1^2 \text{(symmetry)}$

Q

n

n=3

n=2

n=1

Q=1/2

Q=1/3

Q=1/8

Figure 4a

Figure 4b

XBL 7910-4421

The y-axis is labeled $\sum_{n=1}^{n_{max}} \sigma_n^2 / \sigma_1^2$ (symmetry), and the x-axis is labeled Q. The six panels are labeled $n_{max} = 4$, $n_{max} = 7$, $n_{max} = 3$, $n_{max} = 6$, $n_{max} = 2$, and $n_{max} = 5$.
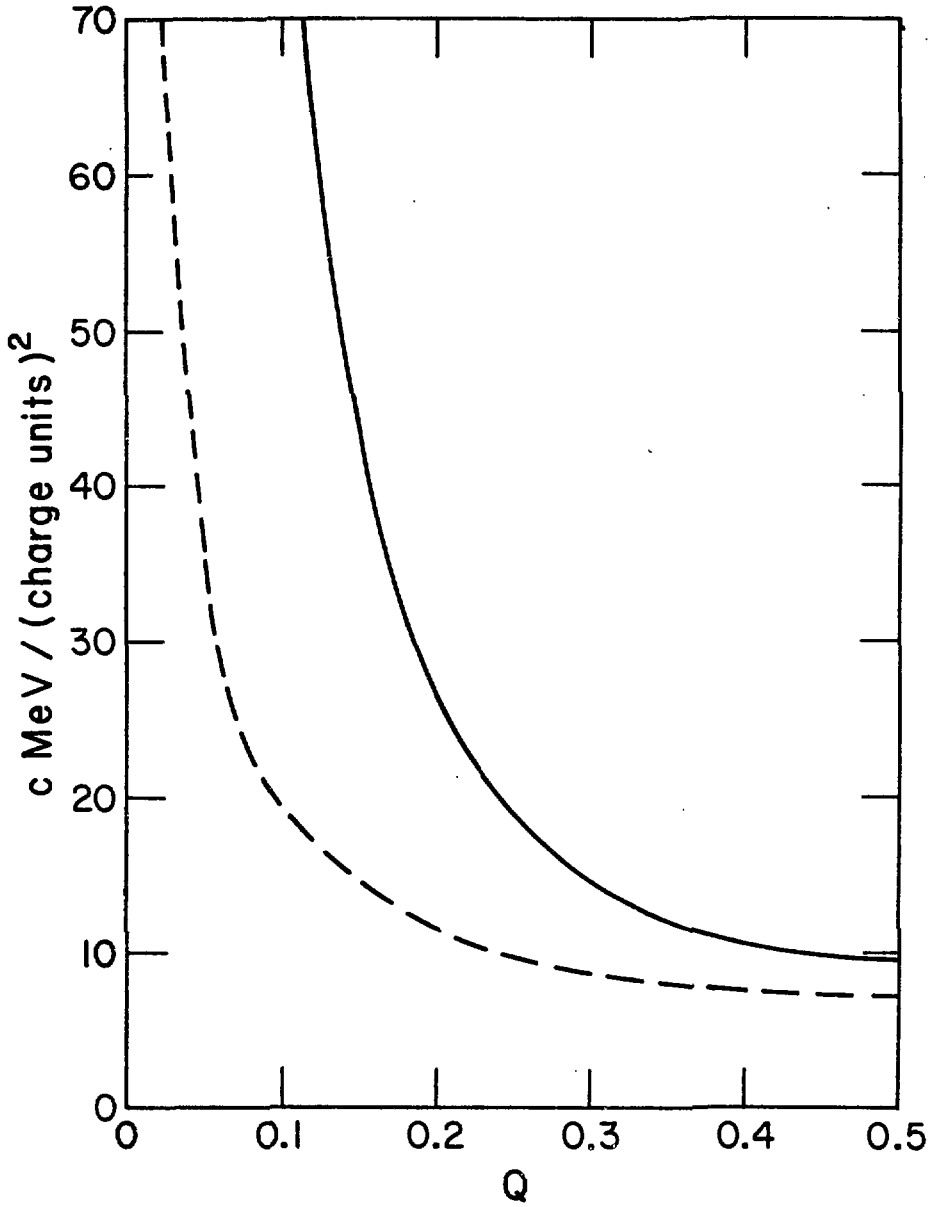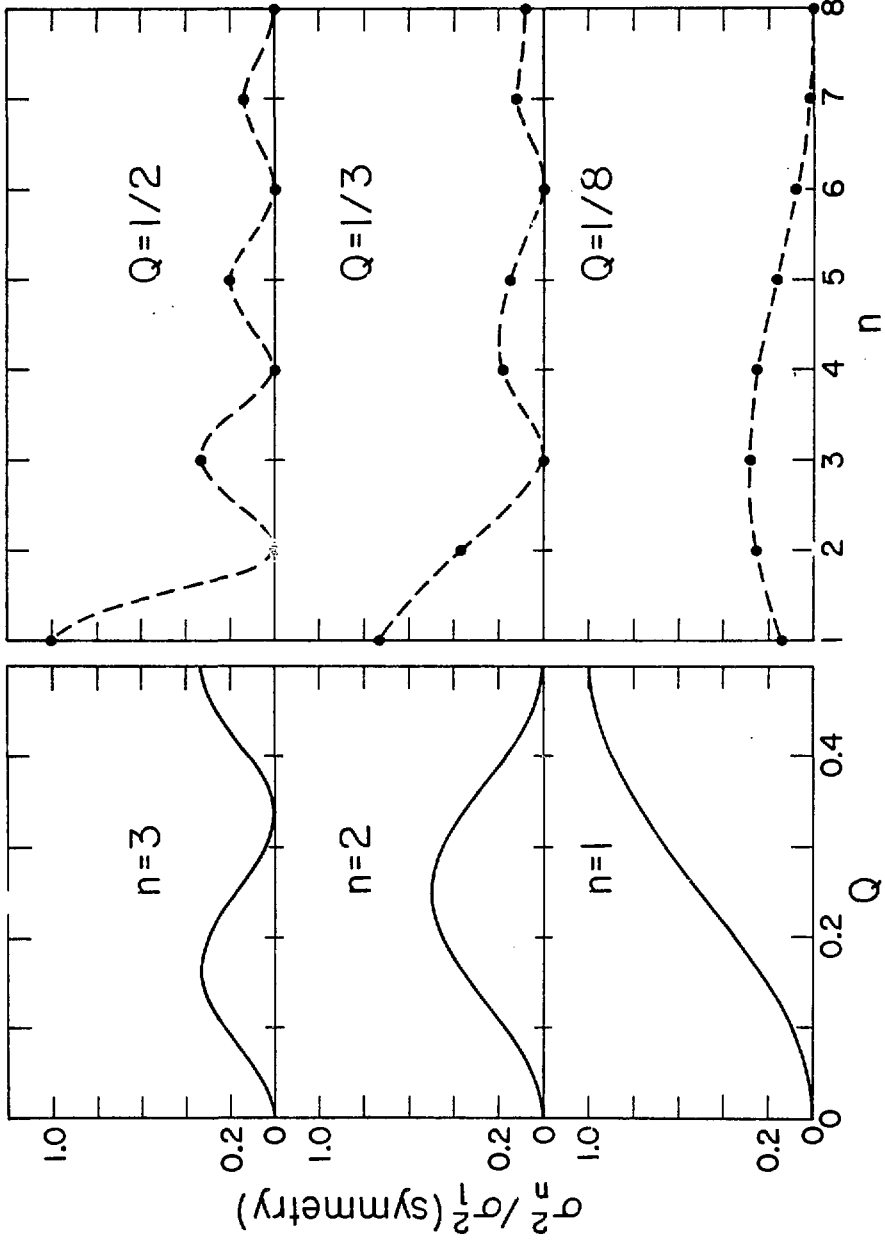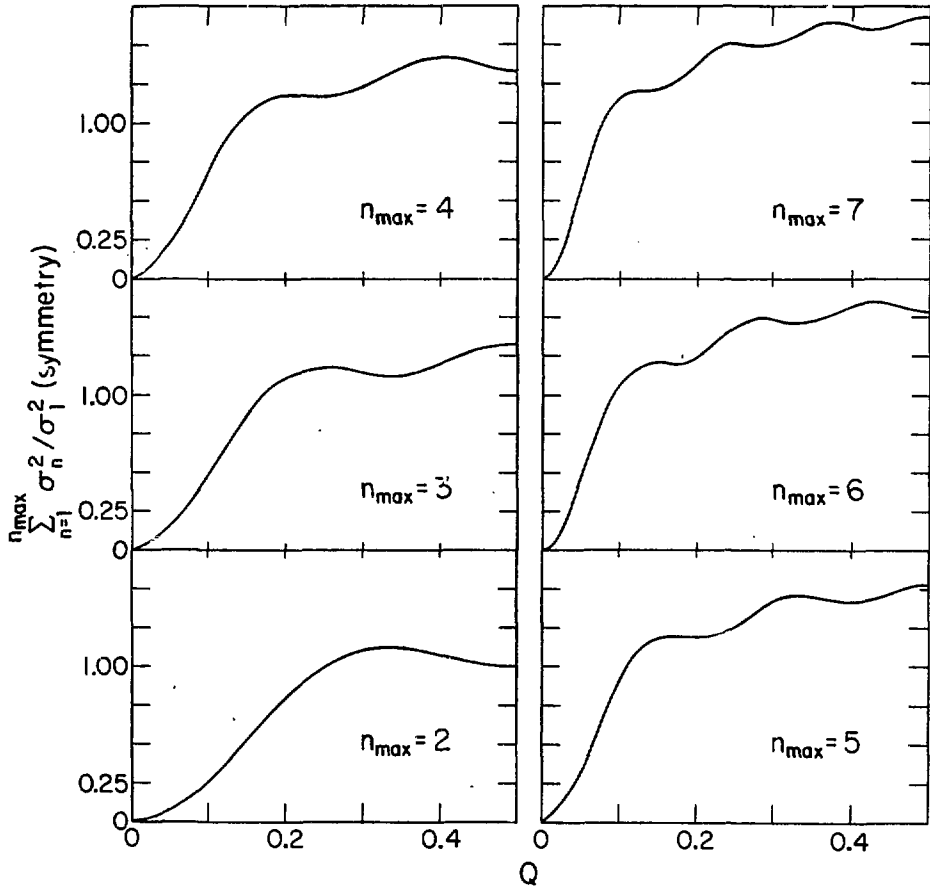
XBL 7910-4420
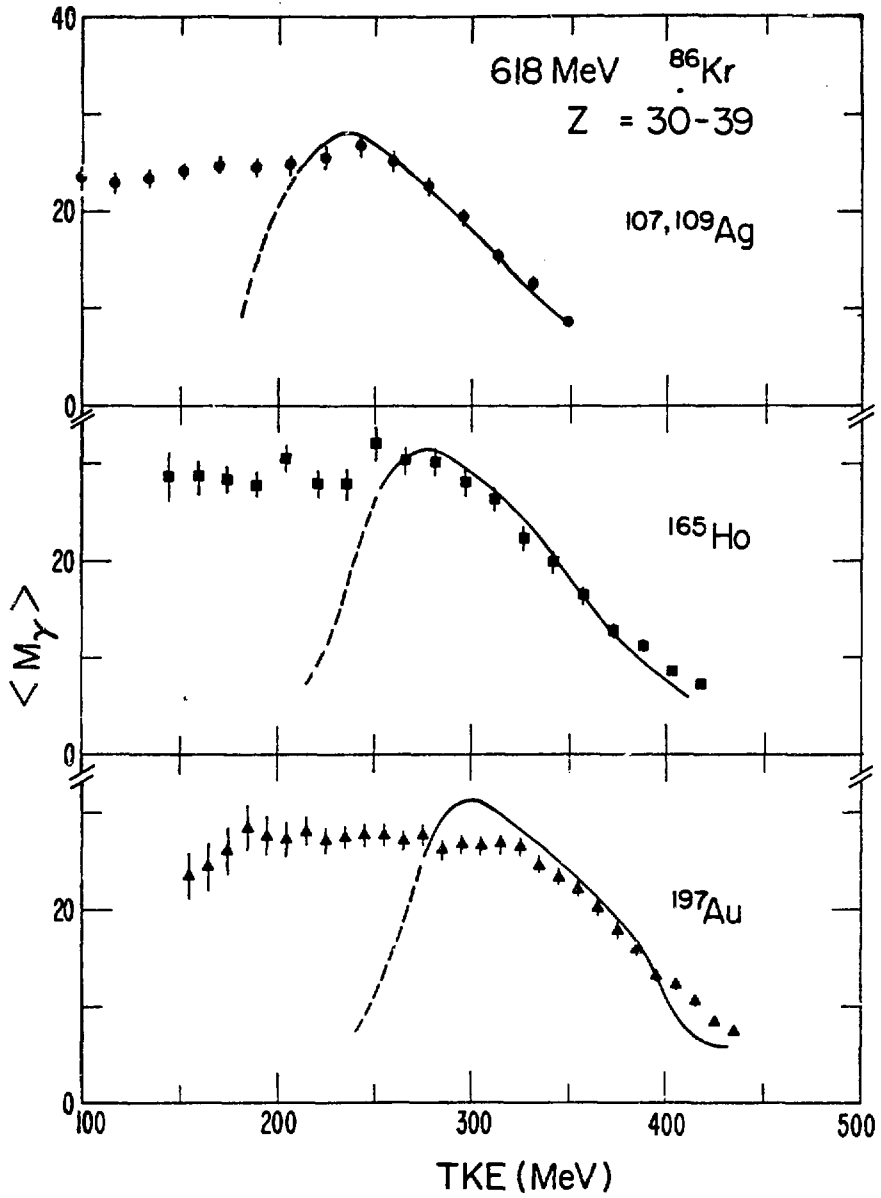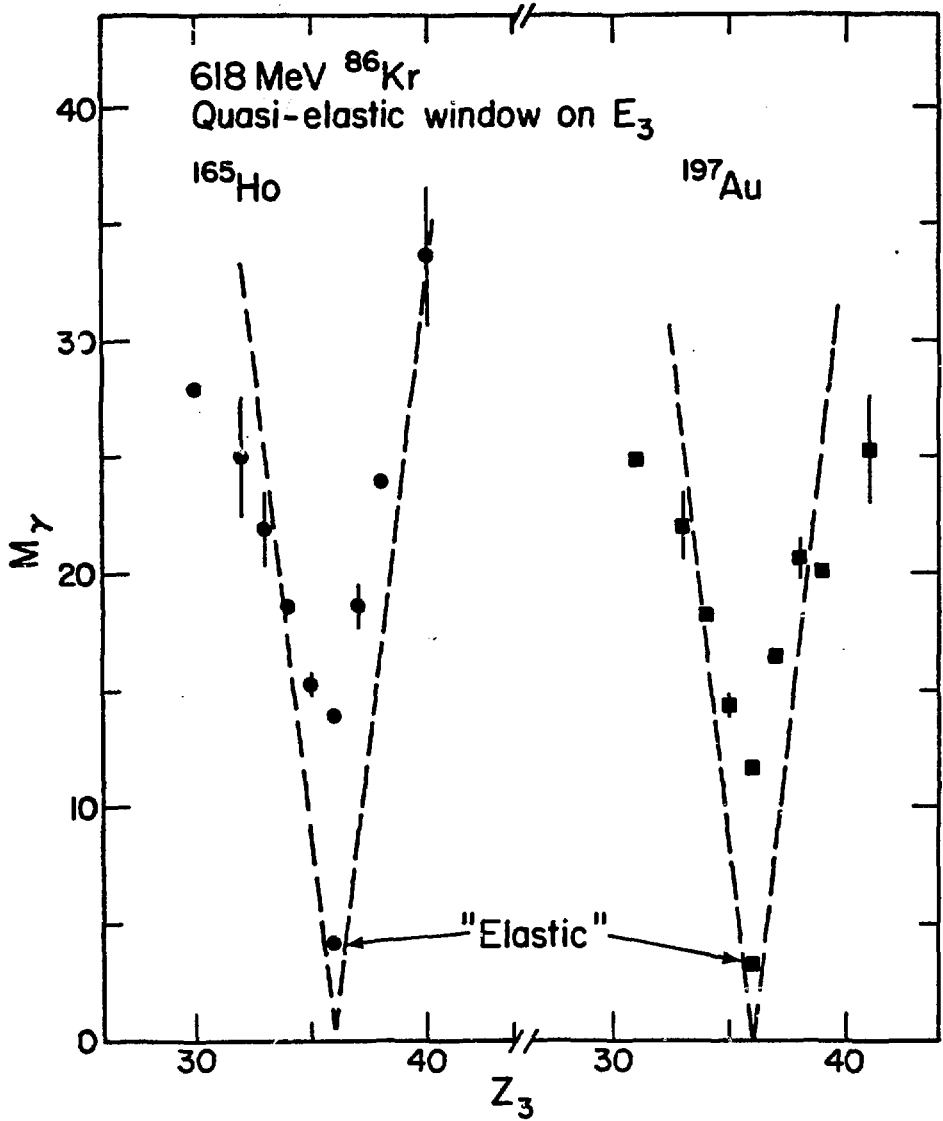
Figure 5
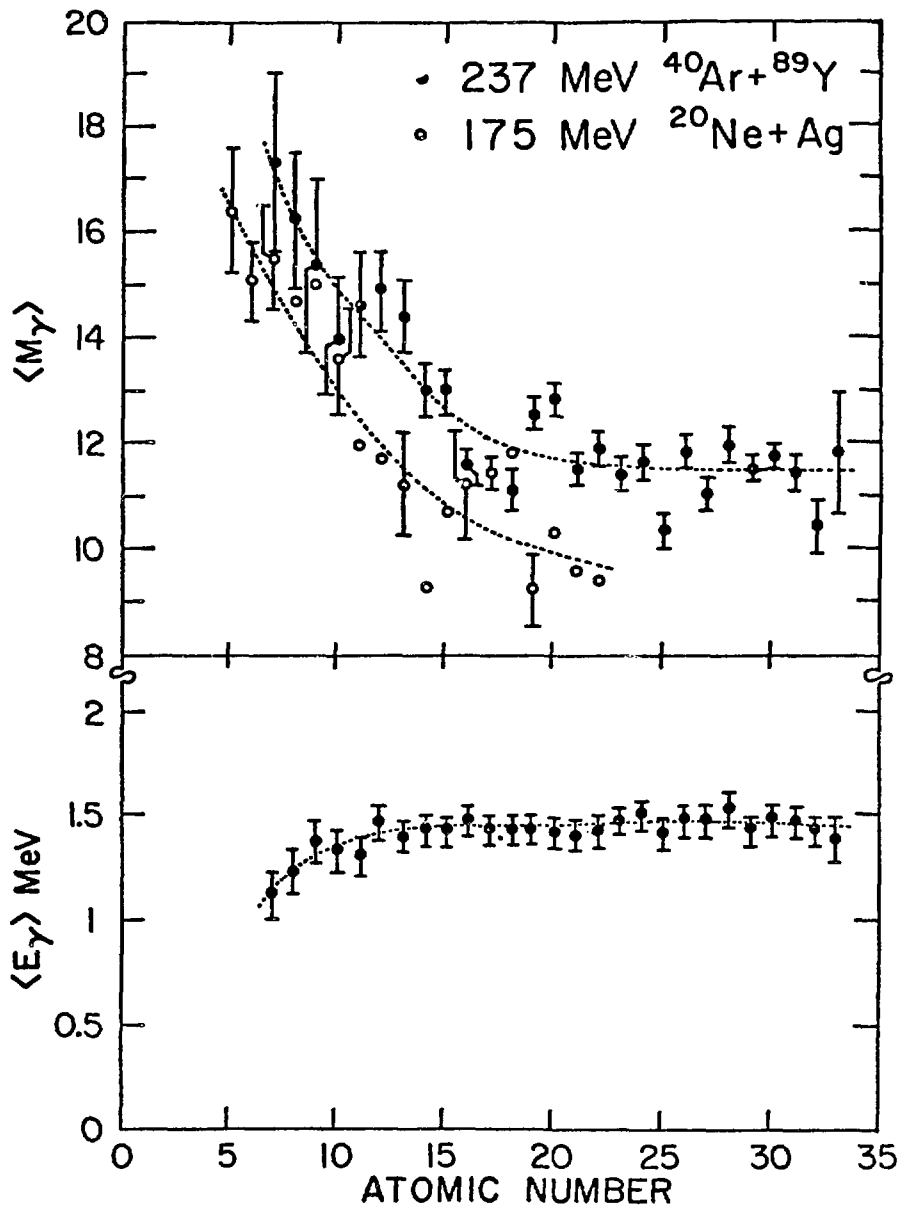
Figure 6
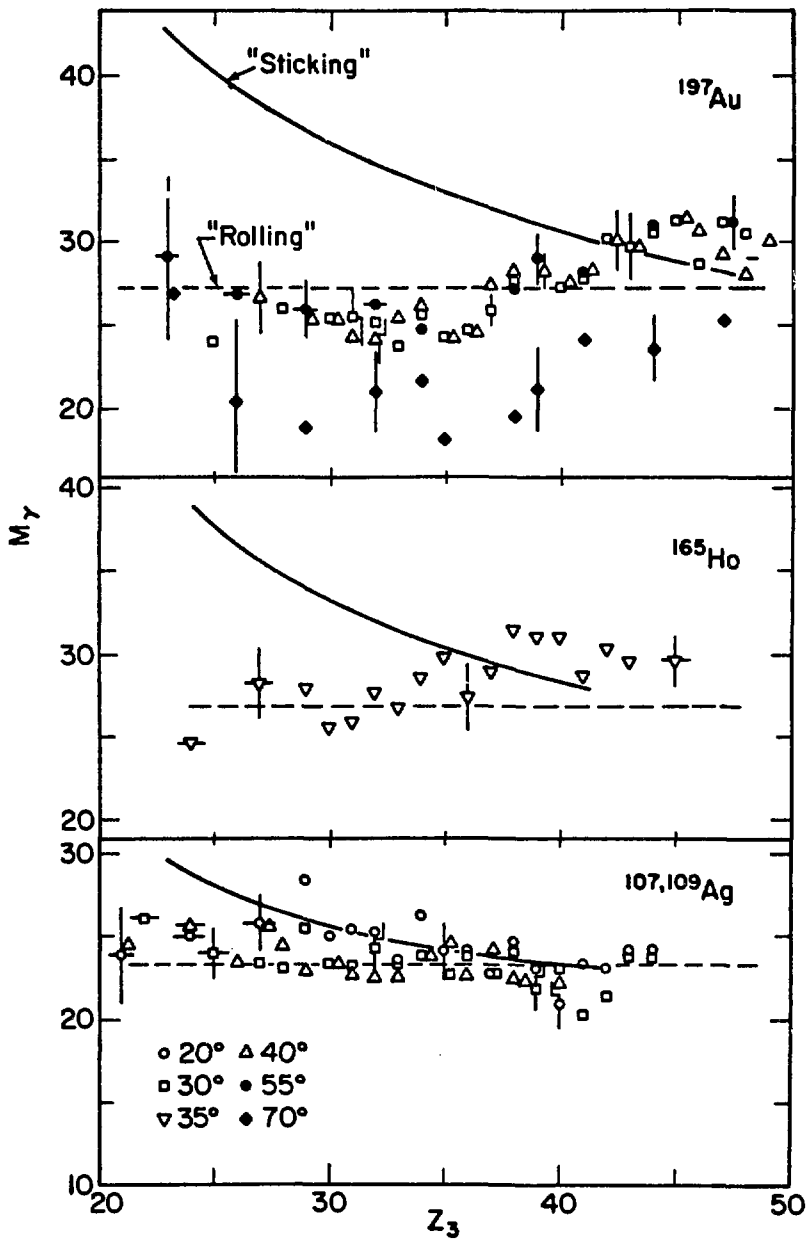
Figure 7

Figure 8

Figure 9
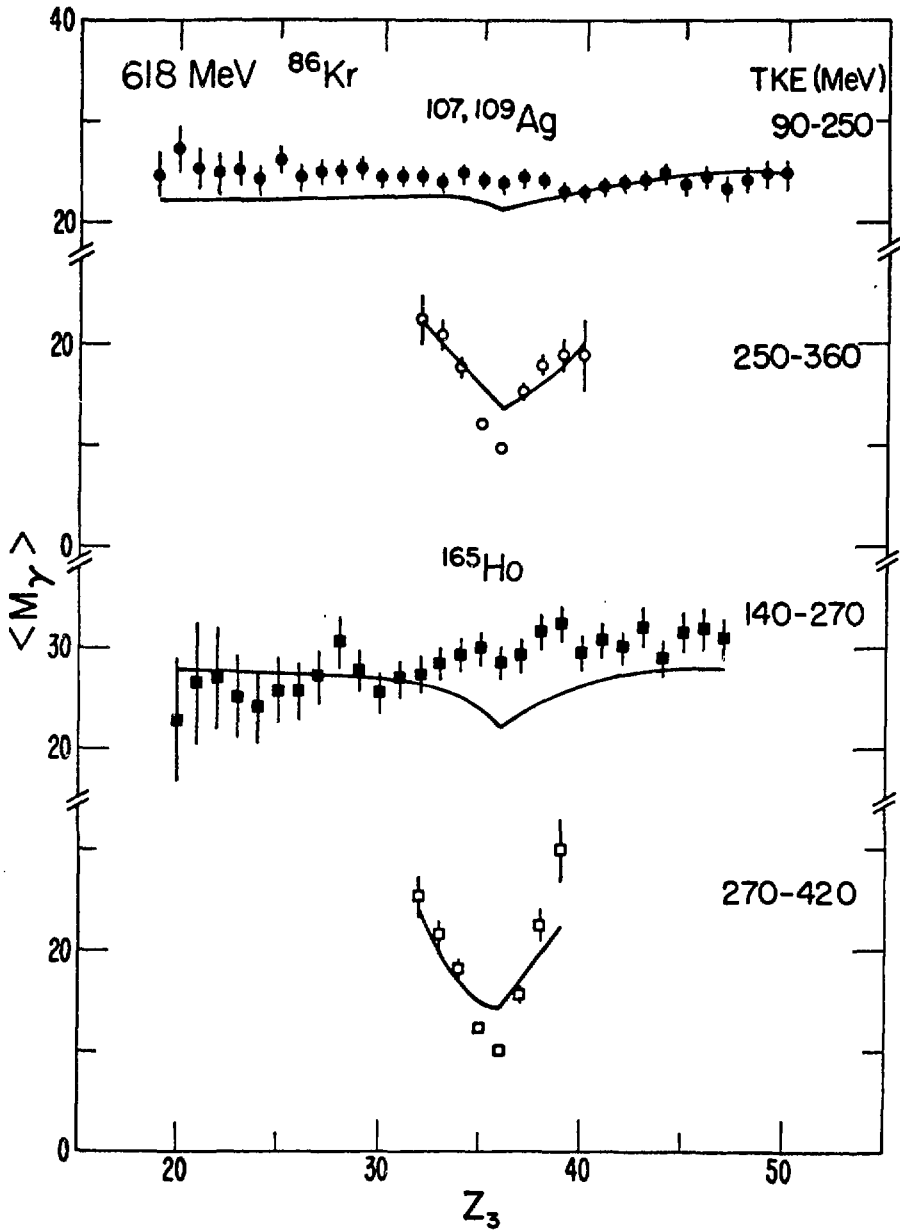
XBL 786-2556

Figure 10
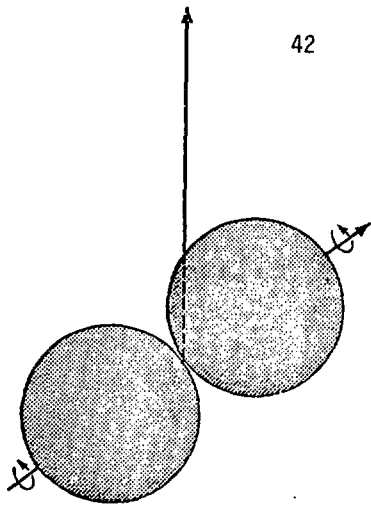
Tilting
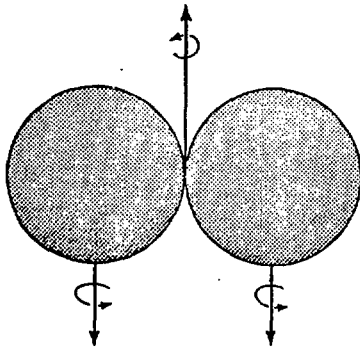
Wriggling
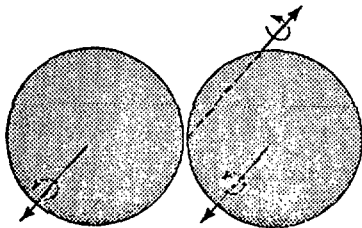
Wriggling ·

XBL 793-824

Figure 11
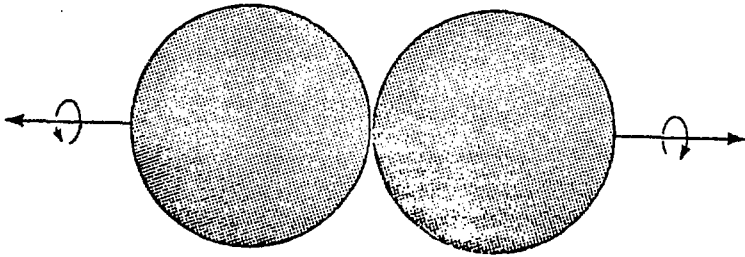
Twisting
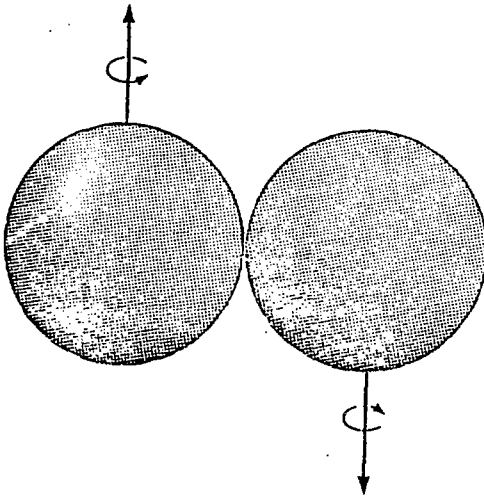
Bending
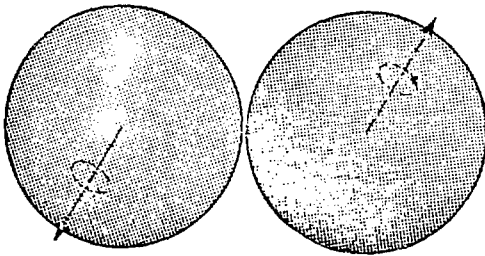
Bending

XBL 79I-206

Figure 12

600 MeV  Kr + Au  sequential fission
In and out-of-plane angular distributions

Figure 13

Figure 14

XBL 783-2453

600 MeV $^{86}$Kr + Au
Sequential fission

$I_{mx} = 40\,\hbar$        $K_0^2 = 100\,\hbar$

$\sigma = 110\,\hbar^2$        $\beta = 0.00194$

FWHM = 54°

$\theta$ (degrees)

XBL 802-275

Figure 15

664 MeV Kr + Ag
α angular distribution

—— No misalignment
– – With misalignment
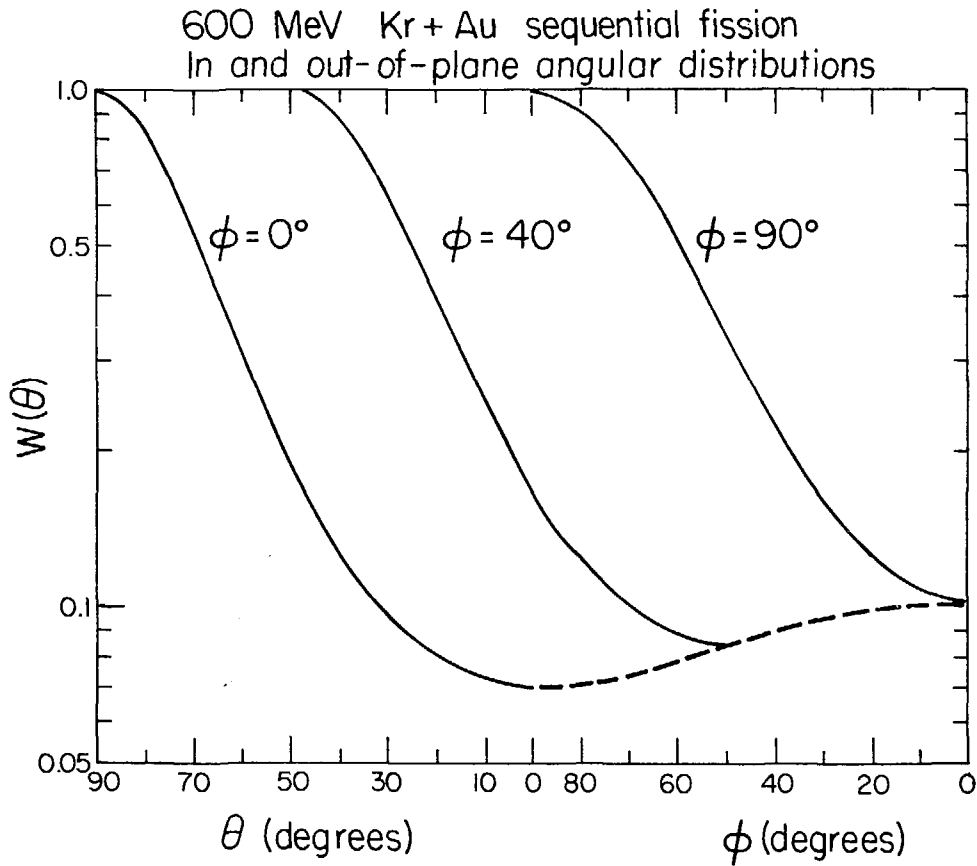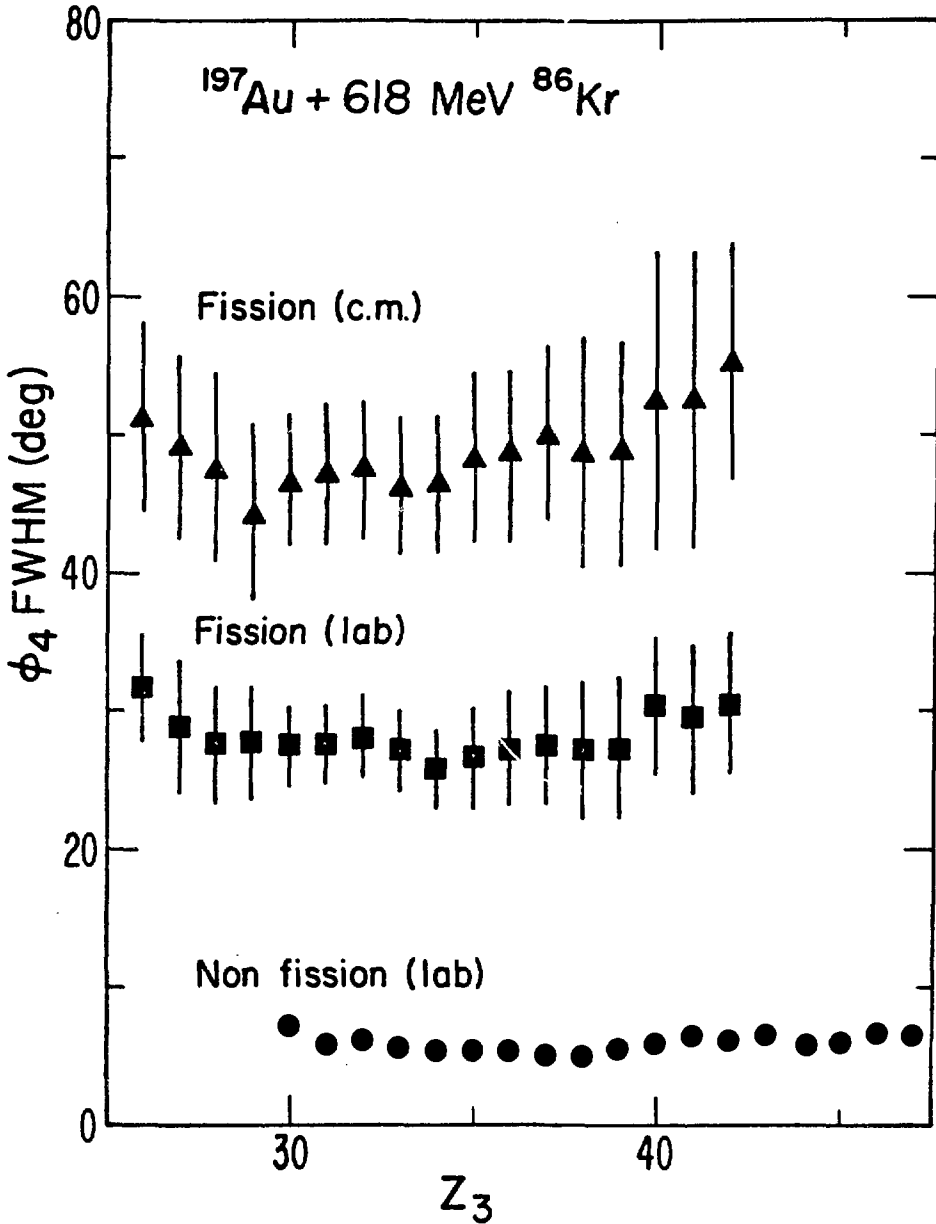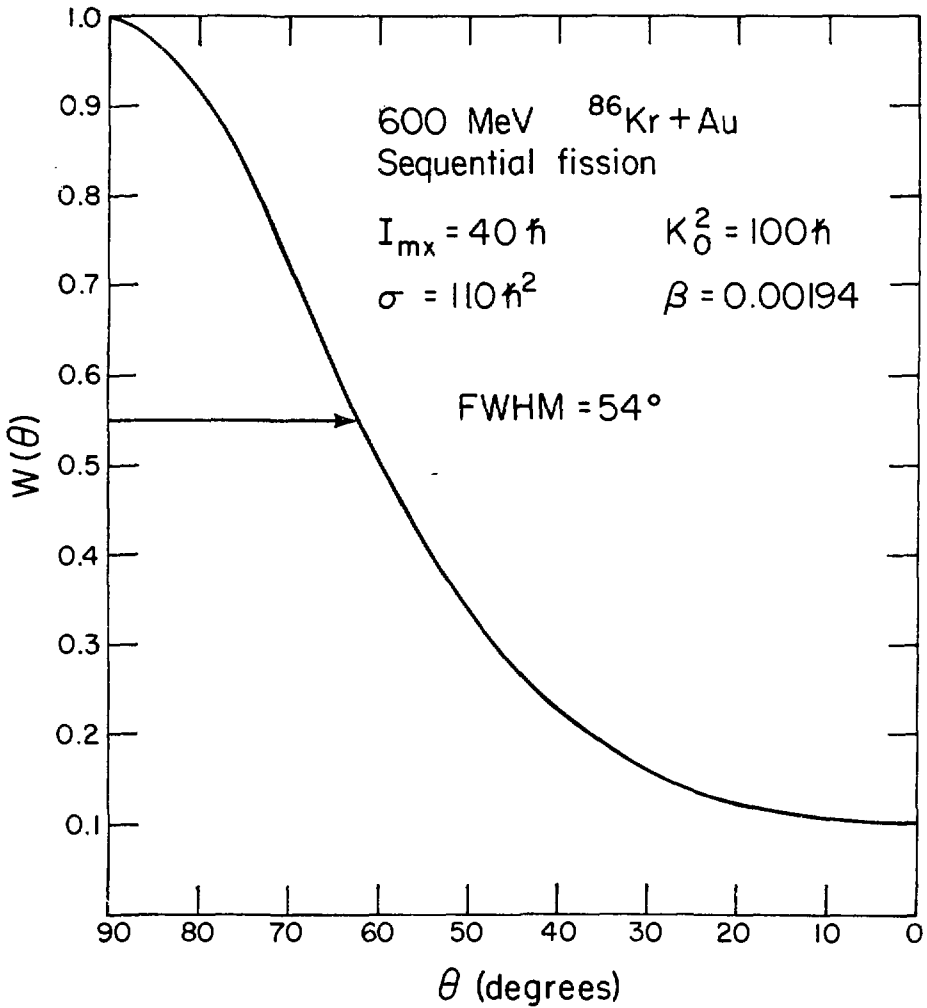
$I = 36\,\hbar$
$\sigma^2 = 68$
$\beta = 0.00137$
$K_0^2 = 365$
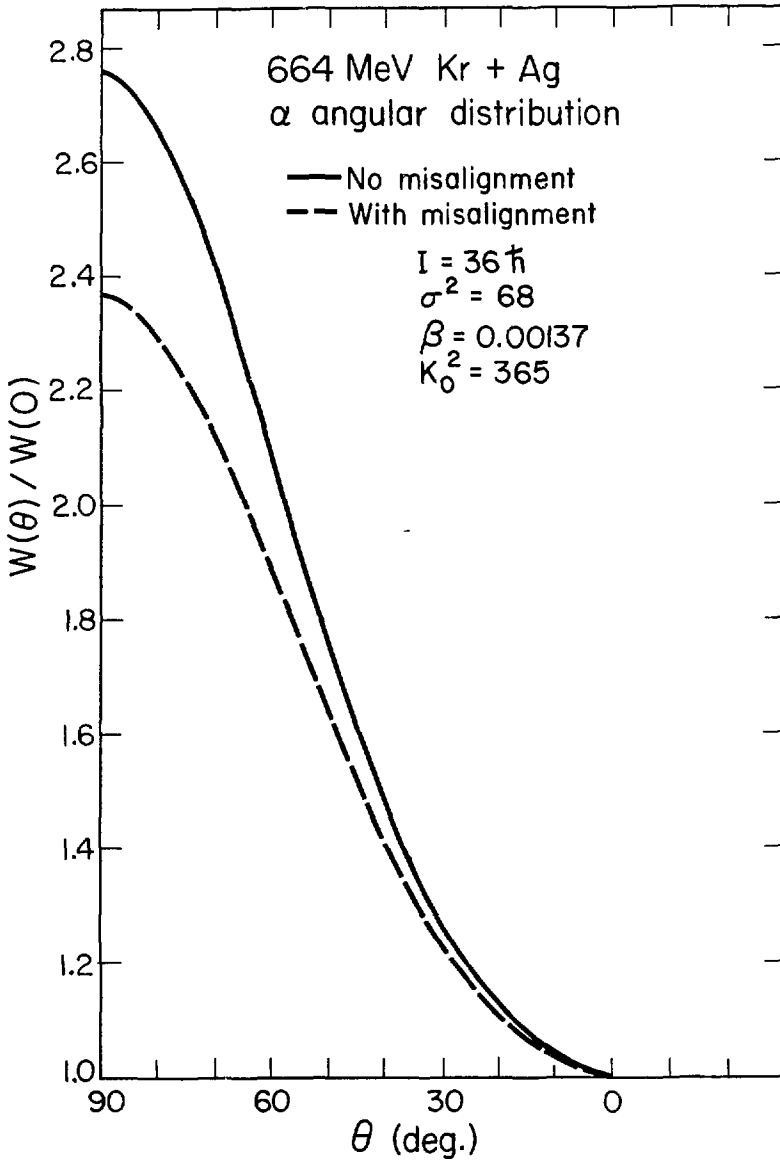
XBL 802–285

Figure 16

$^{84}$Kr (664 MeV) + $^{Nat}$Ag

P($E_\alpha$)

$E_\alpha$ (MeV)
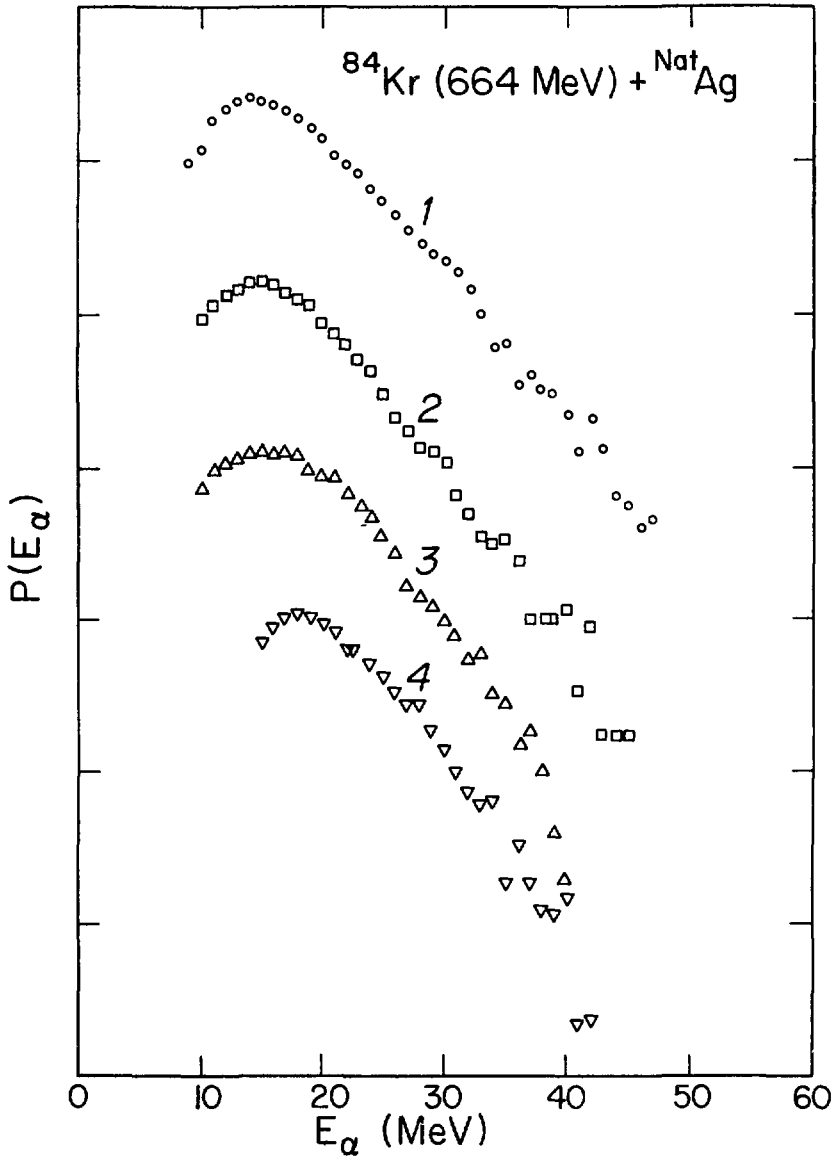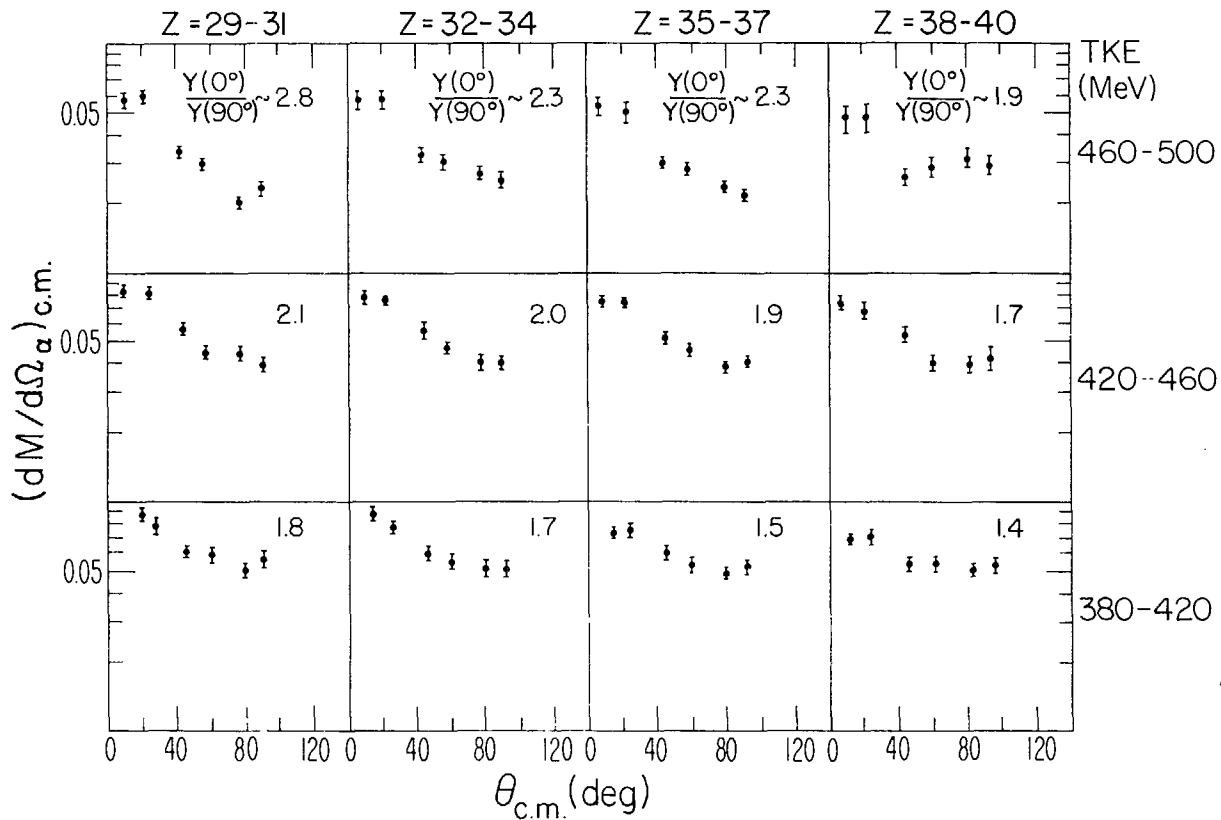
XBL 802-286

Figure 17

Figure 18

$^{Nat}$Ag + $^{84}$Kr  (664 MeV)
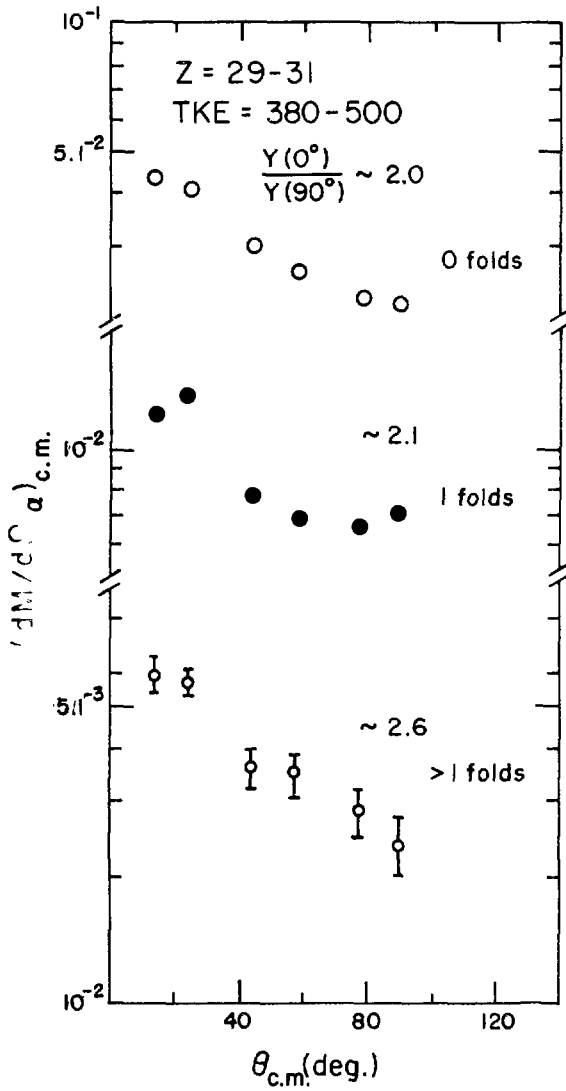


XBL 802-278

Figure 19

XBL 802-279

Figure 20

$^{197}$Au + 1064 MeV $^{136}$Xe

$152 \leq A \leq 172$

$\left(\dfrac{90° \text{ out}}{90° \text{ in}}\right)$  $\left(\dfrac{150° \text{ in}}{90° \text{ in}}\right)$

Q < −280 MeV

−280 MeV < Q < −140 MeV

Q > −140 MeV

R

$E_\gamma$(MeV)  $E_\gamma$ (MeV)
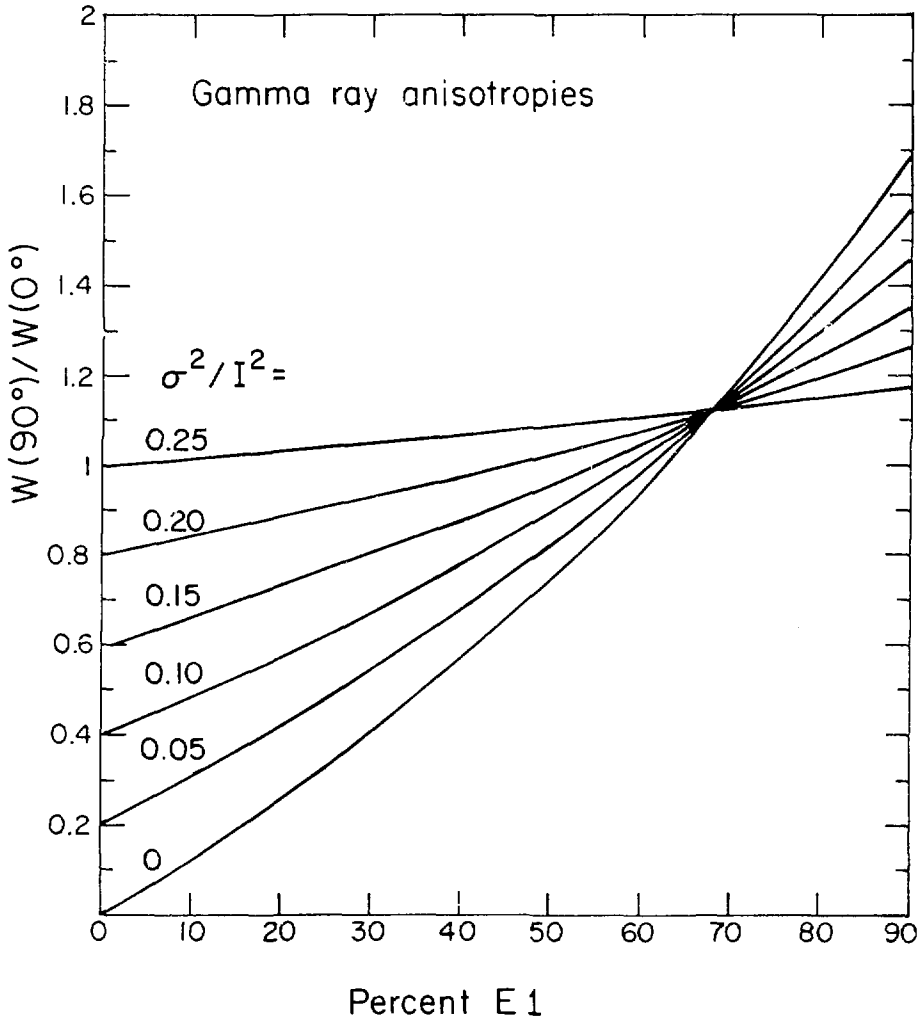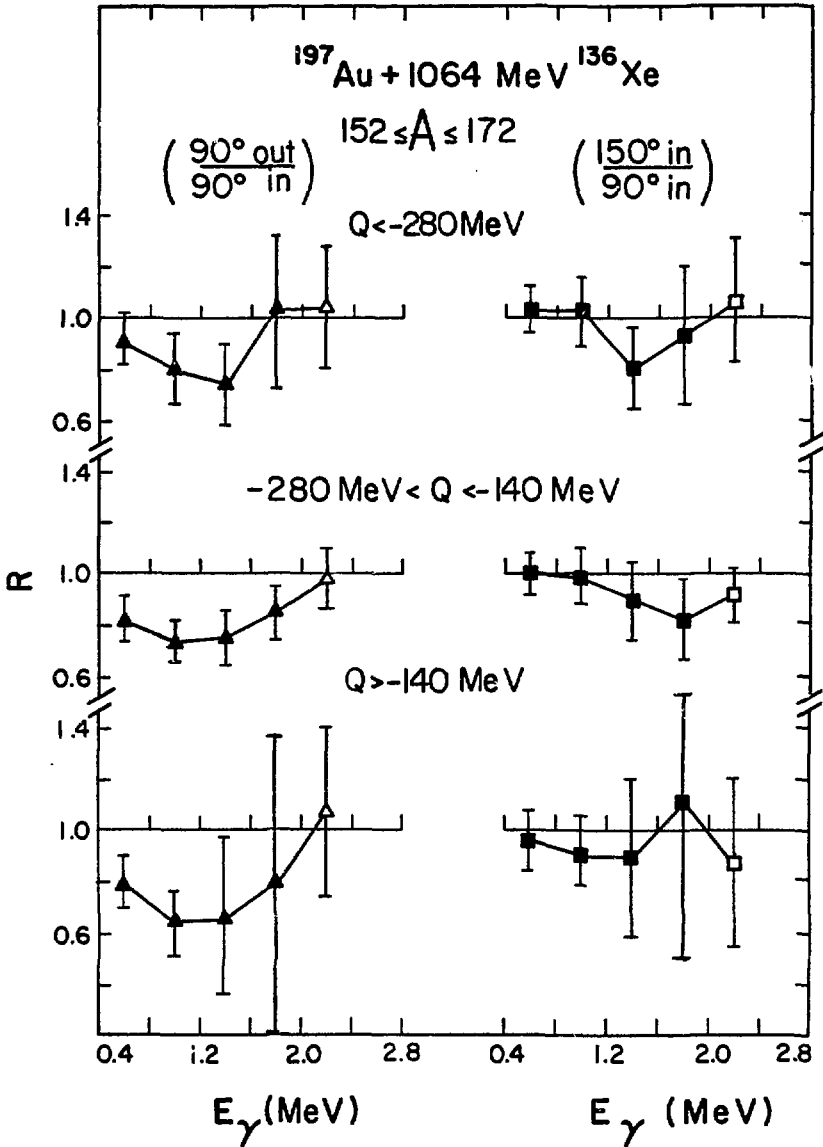
XBL 797−2298

Figure 21

1400 MeV    Ho + Ho

$\theta = 23°$

Counts

$E_\gamma$
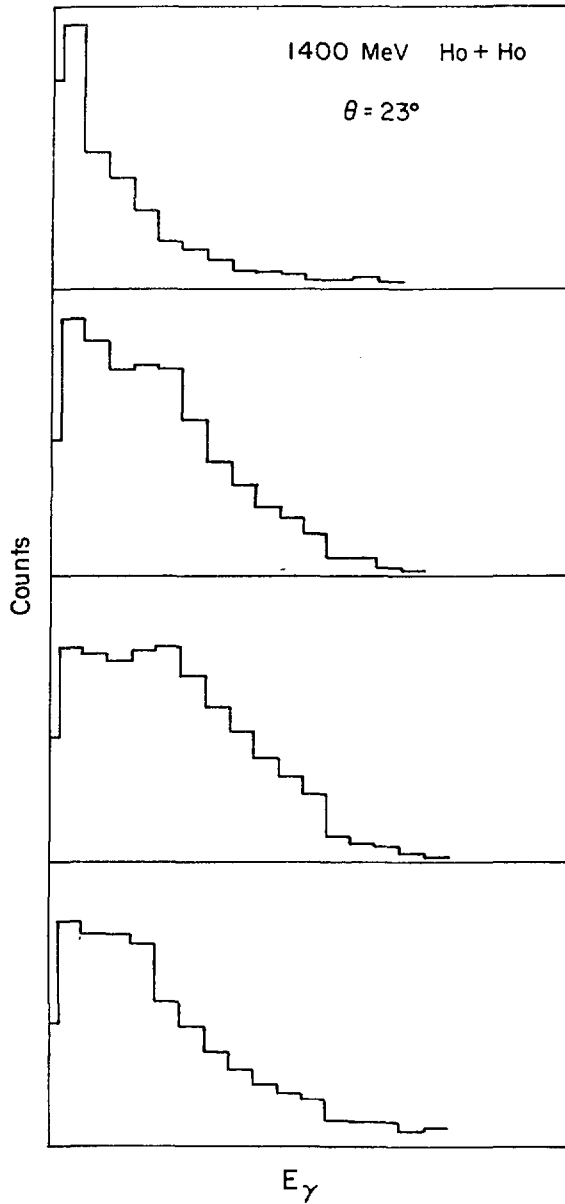
XBL 802 - 282

Figure 22a

1400 MeV Ho + Ho

$\theta = 27°$

Counts

$E_\gamma$
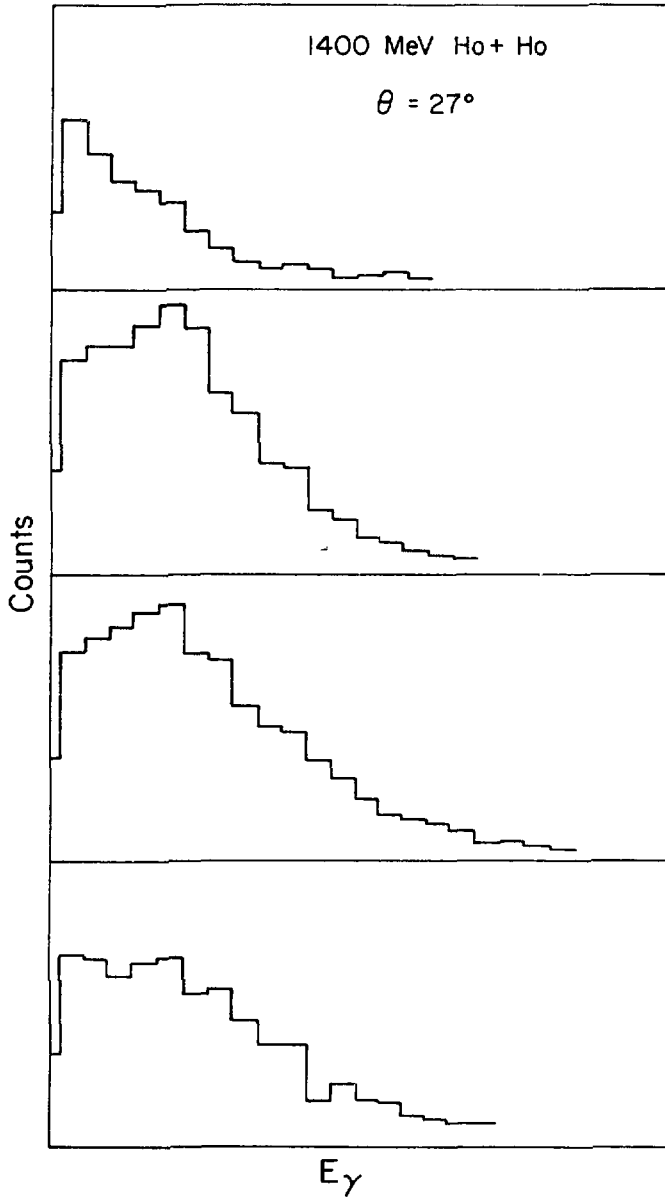
XBL 802-281

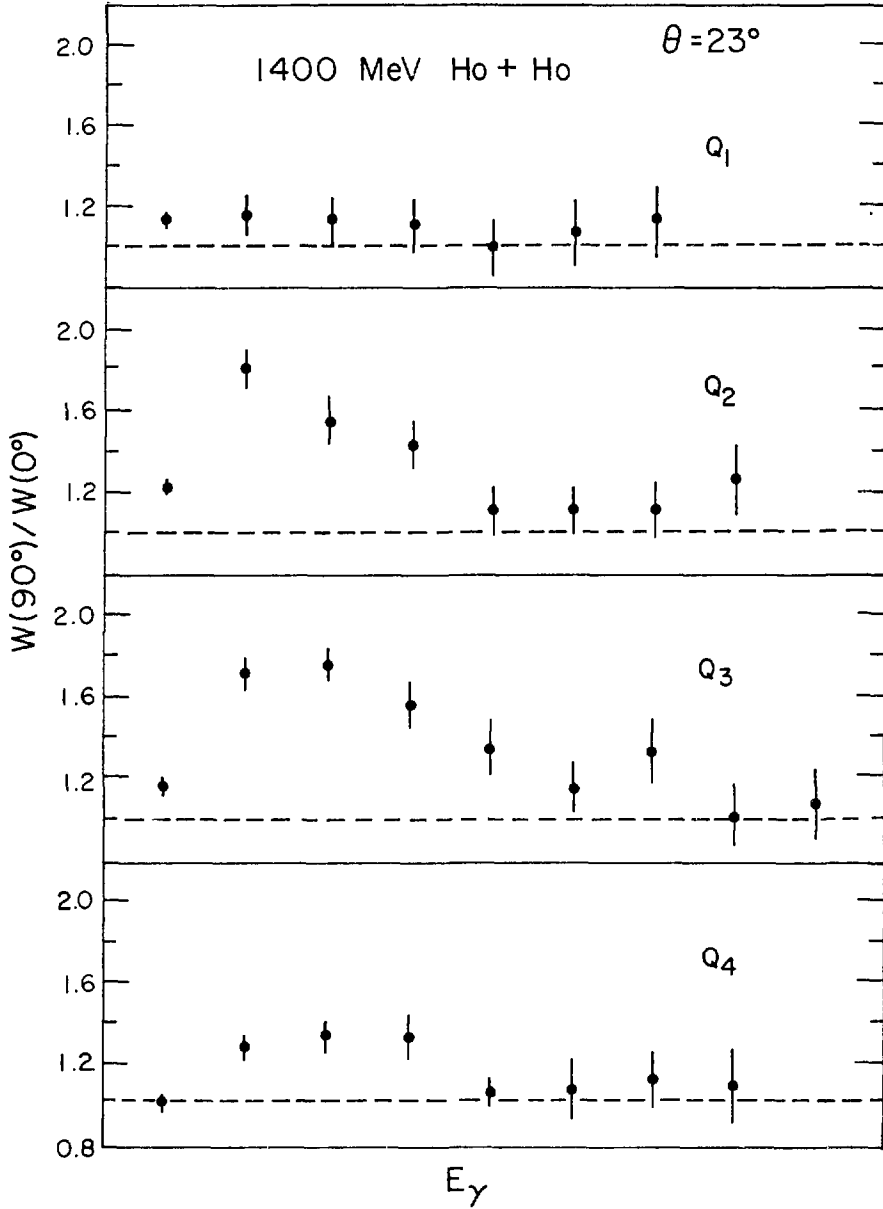Figure 22b

Figure 23a

XBL 802-284

Figure 23b

XBL 802-283